Nanoscale

ROYAL SOCIETY OF CHEMISTRY

MINIREVIEW

View Article Online
View Journal | View Issue

Cite this: *Nanoscale*, 2021, **13**, 17290

Droplet-based nanogenerators for energy harvesting and self-powered sensing

Jianing Dong, Feng Ru Fan * and Zhong-Qun Tian

The energy crisis is a continuing topic for all human beings, threatening the development of human society. Accordingly, harvesting energy from the surrounding environment, such as wind, water flow and solar power, has become a promising direction for the research community. Water contains tremendous energy in a variety of forms, such as rivers, ocean waves, tides, and raindrops. Among them, raindrop energy is the most abundant. Raindrop energy not only can complement other forms of energy, such as solar energy, but also have potential applications in wearable and universal energy collectors. Over the past few years, droplet-based electricity nanogenerators (DENG) have attracted significant attention due to their advantages of small size and high power. To date, a variety of fundamental materials and ingenious structural designs have been proposed to achieve efficient droplet-based energy harvesting. The research and application of DENG in various fields have received widespread attention. In this review, we focus on the fundamental mechanism and recent progress of droplet-based nanogenerators in the following three aspects: droplet properties, energy harvesting and self-powered sensing. Finally, some challenges and further outlook for droplet-based nanogenerators are discussed to boost the future development of this promising field.

Received 17th August 2021,
Accepted 28th September 2021

DOI: 10.1039/d1nr05386h

rsc.li/nanoscale

State Key Laboratory of Physical Chemistry of Solid Surfaces, Collaborative Innovation Center of Chemistry for Energy Materials (iChEM), Tan Kah Kee Innovation Laboratory, College of Chemistry and Chemical Engineering, Xiamen University, Xiamen 361005, China. E-mail: frfan@xmu.edu.cn

Feng Ru Fan

Dr Feng Ru Fan is currently an Associate Professor of Chemistry at Xiamen University. He received his B.S. (2006) and Ph. D. Degree (2013) in Physical Chemistry from Xiamen University under the joint supervision of Prof. Zhongqun Tian and Prof. Zhong Lin Wang. He worked as a Postdoctoral Research Associate in Prof. Galen Stucky's group from 2016 to 2019 at the University of California, Santa Barbara, and in Wenzhuo Wu's group from 2019–2020 at Purdue University. His current research interest focuses on energy harvesting and conversion, triboelectric nanogenerators and self-powered systems, flexible electronics, electrocatalysis, and droplet chemistry.

1. Introduction

Harvesting unused energy directly from the environment is one of the most promising ways to solve the growing energy demand.[1–3] Water covers about 71% of the Earth's surface and absorbs nearly 70% of the solar radiation reaching the Earth's surface. The average annual power of the Earth's water absorbing and releasing energy is as high as 60 trillion kilowatts (10^{15} Watts),[4] which is three orders of magnitude higher than the average global energy consumption by human beings (about 18 billion kilowatts in 2016).[5] As clean and abundant mechanical energy among the different types of water energy, raindrop energy is one of the most potential candidates as a source of energy in daily life. Generally, raindrop energy consists of two types of energy, *i.e.*, kinetic energy converted from potential energy and electrostatic energy generated by triboelectric materials with air or dielectric materials.[6–12] Currently, researchers are studying how to collect both types of energy, especially the latter. Therefore, research on the properties of droplets and understanding droplet nanogenerator systems are crucial. As a classic example, the Kelvin water dropper developed by Lord Kelvin in 1867 realizes droplet energy utilization based on triboelectric, electrostatic induction and electrostatic accumulation principles.[13,14] Inspired by this, to date, the kinetic energy of droplets and electrostatic energy have been fully studied and harvested to achieve self-powered systems (Fig. 1), including droplet piezoelectric nanogenerators

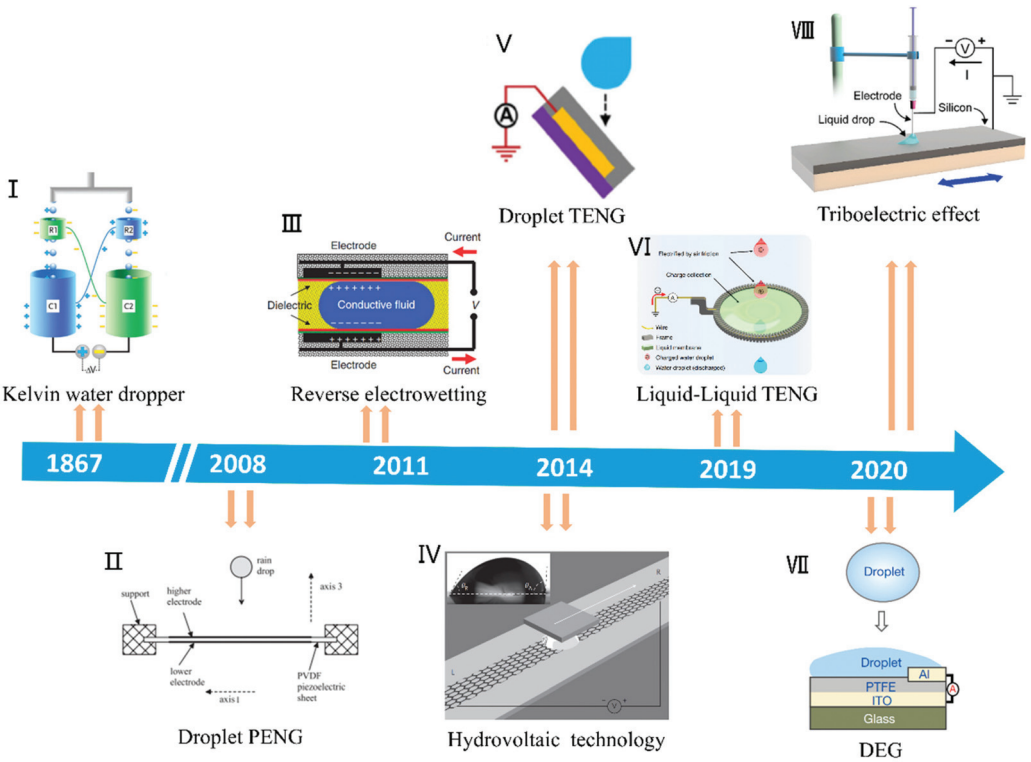

Fig. 1 Timeline of the significant advances of droplet-based nanogenerators. Image (I) has been reproduced from ref. 14 with permission from The Royal Society of Chemistry, Copyright 2013. Image (II) has been reproduced from ref. 15 with permission from IOP Publishing, Copyright 2008. Image (III) has been reproduced from ref. 16 with permission from Nature Publishing Group, Copyright 2011. Image (IV) has been reproduced from ref. 17 with permission from Nature Publishing Group, Copyright 2014. Image (V) has been reproduced from ref. 18 with permission from Wiley-VCH, Copyright 2014. Image (VI) has been reproduced from ref. 19 with permission from Nature Publishing Group, Copyright 2019. Image (VII) has been reproduced from ref. 20 with permission from Nature Publishing Group, Copyright 2020; Image (VIII) has been reproduced from ref. 21 with permission from Elsevier, Copyright 2020.

(droplet PENG), droplet triboelectric nanogenerators (droplet TENG), tribovoltaic effect and hydrovoltaic technology.[15–21] Although various droplet-based nanogenerator structures have been reported, these devices are still based on the interaction between the droplets and substrate materials to achieve energy harvesting or utilization.[22–28] Therefore, it is important to understand the physical and chemical properties of droplets and their motion, as well as the structural design of the device to achieve advanced droplet-based nanogenerators.

Several representative review papers about the applications and rational design of TENG have been previously reported.[29–39] In this review, the latest advances in droplet properties, energy harvesting and self-powered sensing of droplet-based nanogenerators are summarized. Firstly, we discuss the physicochemical properties of droplets, including the pH effect, ion effect, molecular dipole moment and dielectric constant, and the motion of three-dimensional parameters, including the Weber number (We), Reynolds number (Re) and Ohnesorge number (Oh) during power generation. Next, the design principles of the energy harvesting device are described, which are categorized as droplet triboelectric nanogenerators, tribovoltaic effect, hydrovoltaic technology and other promising technologies. Then, some advanced self-powered sensing systems based on droplet nanogenerators are reviewed, including physical sensing and chemical sensing. Finally, the remaining challenges and future perspectives of energy harvesting through droplet-based nanogenerators are discussed.

2. Droplet properties for nanogenerators

pH and ion effect

The pH environment of droplets not only has a great influence on the efficiency of energy harvesting, but also has a significant effect on the charged polarity of the contact electrification (CE).[40–46] As is known, polytetrafluoroethylene (PTFE) occupies the most negative position in the friction sequence, and thus is widely used as a material for the construction of droplet-based nanogenerators.[47–53] In recent studies (Fig. 2a), pH ≈3 has been reported as the critical threshold in the system of water and PTFE interaction. When the pH of the droplet exceeds 3, the droplet is positively charged and PTFE is negatively charged. With an increase in the pH value, the amount of CE charges increases. On the contrary, when the pH value is lower than 3, the droplet shows a negative polarity, while the PTFE substrate

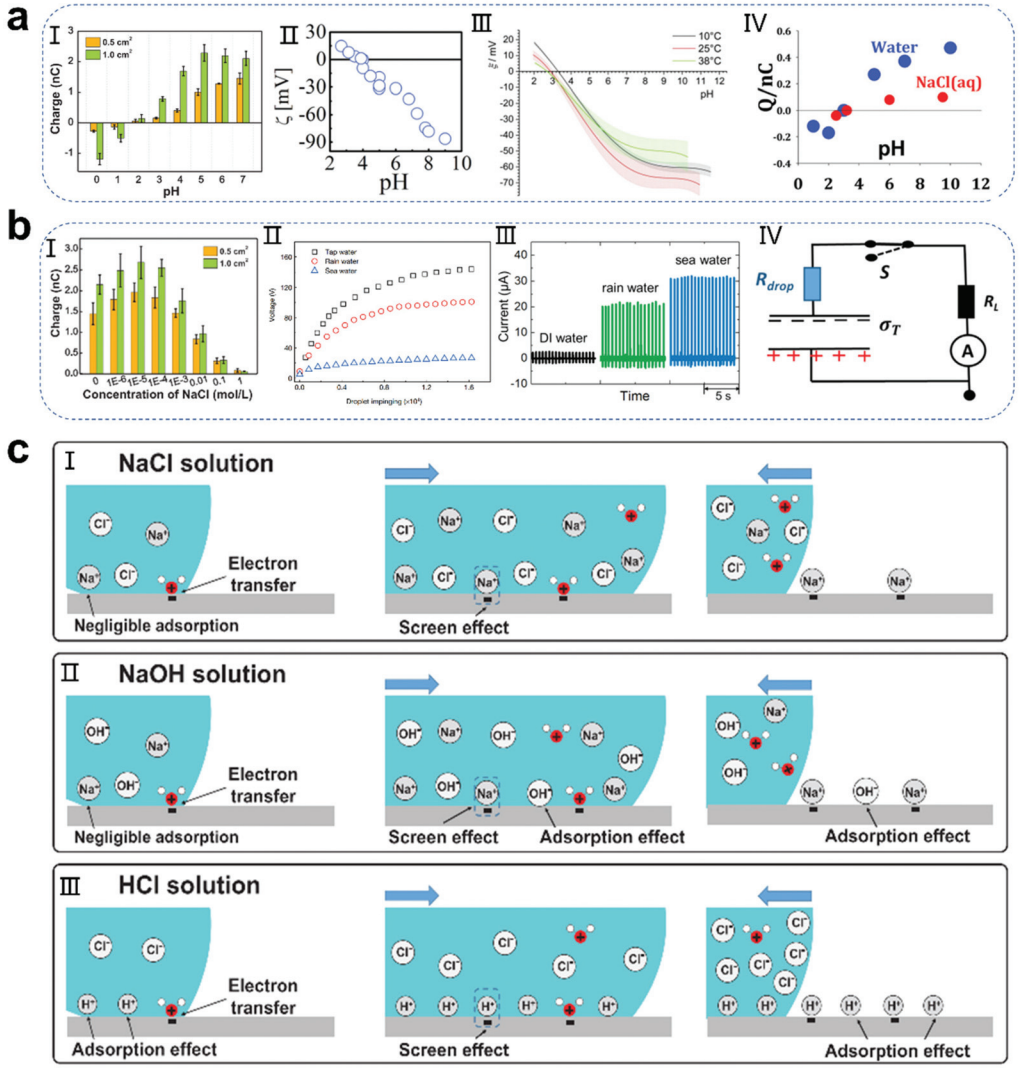

Fig. 2 Influence of the pH and ionic effect of droplets on the performance of the generator and schematic of the related mechanisms. (a) Change in PTFE surface charge induced by the pH effect of droplets. Image (I) has been reproduced from ref. 40 with permission from Wiley-VCH, Copyright 2020. Image (II) has been reproduced from ref. 41 with permission from The Royal Society of Chemistry, Copyright 2017. Image (III) has been reproduced from ref. 42 with permission from The Royal Society of Chemistry, Copyright 2020. Image (IV) has been reproduced from ref. 43 with permission from Wiley-VCH, Copyright 2004. (b) Change in PTFE surface charge induced by the ionic effect of droplets. Image (I) has been reproduced from ref. 40 with permission from Wiley-VCH, Copyright 2020. Image (II) has been reproduced from ref. 20 with permission from Nature Publishing Group, Copyright 2020. Images (III and IV) have been reproduced from ref. 62 with permission from Wiley-VCH, Copyright 2020. (c) Mechanism of CE between different droplets and PTFE films: ionic effect (I) and pH effect (II and III). These figures have been reproduced from ref. 40 with permission from Wiley-VCH, Copyright 2020.

shows a positive polarity. This phenomenon is consistent with the extensive literature on the electrokinetic potential of PTFE.[40–46] Furthermore, Mugele and co-workers calculated the theoretical charge of the surface potential of PTFE in the absence of salt solutions, where at pH = 6, the surface potential of PTFE is −40 mV, and the surface charge density can be calculated from the diffuse part of the electric double layer using the ε value and the Gouy–Chapman relation as follows:[41]

$$\sigma = \sqrt{8\varepsilon\varepsilon_0 RTc}\sin h\left(\frac{e\varepsilon}{K_B T}\right) \quad (1)$$

where R is the universal gas constant and $c \approx 10^{-6}$ mol L^{-1} is the ion concentration in near neutral water without any added salt. The calculation results showed that the theoretical surface charge of PTFE is slightly larger than the actual charge. Recently, Wang and co-workers further explained this phenomenon.[40] Specifically, when the concentration of hydrogen ions in solution exceeds a certain concentration (about 0.01 mol L^{-1}), because of the preferential effect of electron transfer at the solid–liquid interface, the hydrogen ions are further adsorbed to produce the shielding effect of free ions, resulting in a charge reduction or even inversion (Fig. 2c-II and III). It is worth noting that for different surroundings

between various liquids and solids, the critical pH value will change, which needs to be further explored.[54–61]

Additionally, the concentration and species of ions in droplets also strongly affect the output performance of droplet-based nanogenerators. Although most papers have reported the influence of ionic salt on the power generation performance, the relevant mechanism has not been fully discussed due to the need to discuss the influence of ionic strength on the interface at the molecular level.[20,62–69] Preliminarily, based on a simple phenomenological argument, researchers proposed the potential influencing reasons. Negri and co-workers carried out a correlation analysis from the perspective of salt solution solvation.[42] When an unhydrolyzed salt is added to an aqueous solution, water molecules participate in the solvation of the cations and anions (solvated water), thereby reducing the activity of water at the solid–liquid interface. Considering that a droplet contains a small amount of water molecules, this effect is more obvious on the surface of the droplet than that on the bulk water, which will lead to a decrease in the amount of free water and charge transfer. Simultaneously, Wang and co-workers also found that as the salt concentration increases, the amount of charge transferred at the solid–liquid interface first increases and then decreases (Fig. 2b-I).[40] This is because the ultra-low ion concentration or pure water cannot completely promote the ion transfer at the liquid–solid interface. A small amount of salt solution can support the ion transfer process to increase the amount of charge transferred at the solid–liquid interface, thus resulting in a large electrical output. In contrast, as the concentration of the salt solution further increases, the cations will be preferentially adsorbed on the substrate and produce a shielding effect to hinder the charge transfer (Fig. 2c-I). Furthermore, Wang and co-workers found that the voltage output of droplet-based nanogenerators is related to the type of water droplets used, and the performance decline follows the order of tap water > rain water > sea water, where sea water has the highest salt content (Fig. 2b-II).[20] Nevertheless, there are also reports with the opposite conclusions. Mugele and co-workers reported the fabrication of a charge trapping droplet nanogenerator (CTEG).[62] In the case of the CTEG, the current density further increases with an increase in the salt concentration, which is due to the decrease of the droplet resistance in series (the measured conductivities of DI water, rain water and sea water are 0.038 μS cm^{-1}, 33.0 μS cm^{-1}, and 67.2 mS cm^{-1}, respectively), leading to an increase in the overall current density (Fig. 2b-III and IV). Therefore, the influence of the ionic strength of droplets on the power generation performance is a complex subject. This requires not only the interaction between salt ions and water molecules to be understood at the molecular level, but also the specific structure of the device needs to be considered.

Molecular dipole moment and dielectric constant

When contact electrification occurs in the components at the solid–liquid interface, regardless of the transfer of charged substances (electrons, ions or other species), the ability of the solid and liquid to hold charge determines the output performance of the whole droplet nanogenerator.[70–74] In the past, numerous studies on the selection and modification of solid substrate materials have been reported, and many tutorial reviews have also been summarized.[29–39] However, there are relatively few studies on the properties of liquids for nanogenerators, although they are crucial in playing the other role that affects the performance of the entire device. The polarity of the molecules in a liquid determines its ability to solvate electrons or other charged substances. The larger the polarity of the molecules, the more stable the solvated charged substances.[75–79] Normally, the polarity of the molecules in a liquid can be represented by two main characteristics, *i.e.*, the dipole moment and dielectric constant (Fig. 3a).[80,81] The dipole moment of a molecule is the product of the distance r between the positive and negative charge centers and the amount of charge q carried by the charge centers, which can be calculated using the following formula (Fig. 3a-I):

$$\mu = r \times q \quad (2)$$

where μ is the dipole moment of the molecule. The dipole moment is measured in Debye unit (D). 1 Debye is approximately 3.33×10^{-30} C m. Molecules typically have dipole moments of around 1 D. Generally, solvent molecules with a larger dipole moment are more prone to solid–liquid contact electrification and achieve a greater degree of charge transfer, thereby providing a higher energy output. The dielectric constant is also an important parameter for droplets, which is similar to the solid material selection of the droplet nanogenerator (Fig. 3a-II). Liquid droplets with a large dielectric constant show capacitive behavior to accommodate more charges. In previous reports, water, which has a high polarity, exhibited high power generation performances, but there are a few reports on other liquid power generation devices. In a recent work, Soh and colleagues achieved the charging of various organic liquids by sliding them across a rubbed surface.[75] The results showed that the charge per unit mass of the organic liquids is closely related to their dipole moment and dielectric constant. Among the organic liquids, diethyl ether has the highest dipole moment and dielectric constant, and thus it presents the largest amount of charge, which is close to 90 nC g^{-1}. However, diethyl ether has high volatility and toxicity, and thus cannot be used for stable droplet power generation. Recently, Nakanishi and co-workers reported a liquid porphyrin as a liquid electret.[82] The surface potential of the liquid was as high as −330 V after the corona charging treatment. When used as a liquid electret device, although its average output voltage was delayed during the initial 12 h, it was stable for more than 1044 h (43.5 days). However, this liquid electret has high viscosity and a complicated synthetic process, which is not suitable for large-scale use in convenient droplet-based nanogenerators. Therefore, the discovery and further design of highly polar, environmentally friendly and safe droplet carriers is a promising research field for the development of liquid–solid and liquid–liquid nanogenerators.

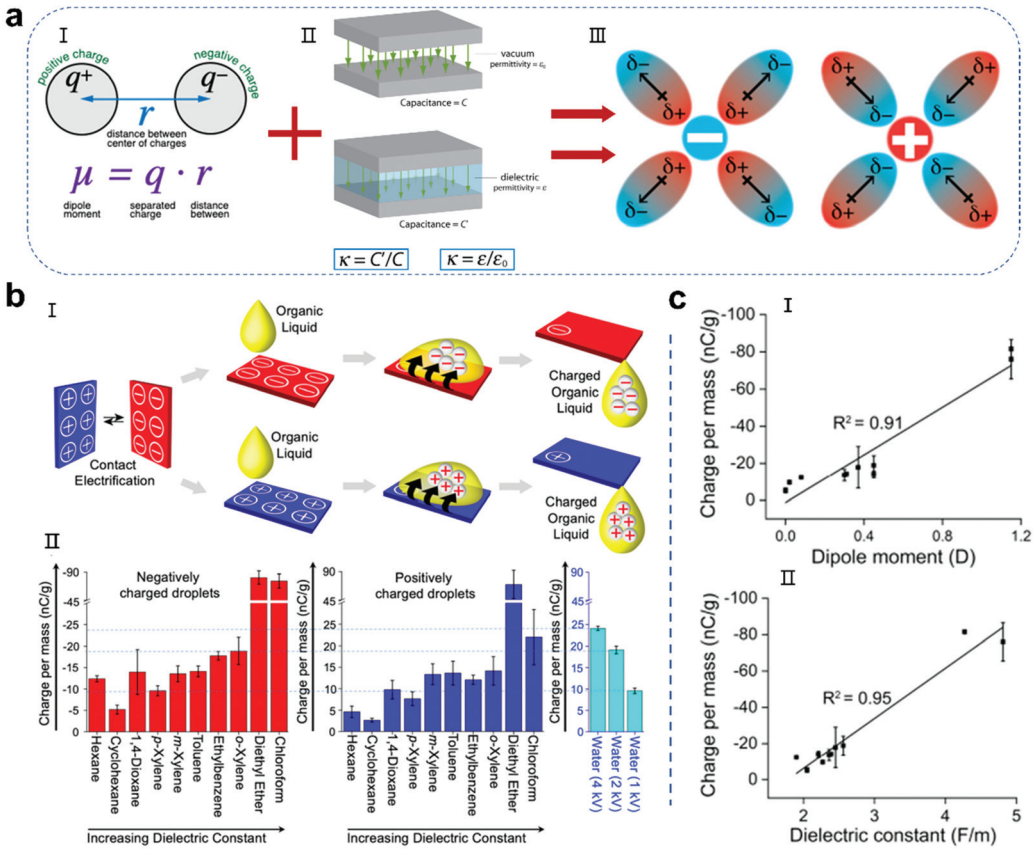

Fig. 3 Influence of the molecular dipole moment and dielectric constant on the amount charges of droplets. (a) Molecular dipole moment and the dielectric constant stabilizing the charged species in the droplet. Images (I and II) have been reproduced from ref. 80 and 81 with permission from the websites, respectively. Image III has been reproduced from ref. 75 with permission from the American Chemical Society, Copyright 2020. (b) Organic droplets charged by sliding on CE surfaces (I) and charge per mass of corresponding organic liquids (II). These figures have been reproduced from ref. 75 with permission from the American Chemical Society, Copyright 2020. (c) Correlation between the amount of negative charge gained by the organic liquids at saturation: dipole moment (I) and dielectric constant (II). These figures have been reproduced from ref. 75 with permission from the American Chemical Society, Copyright 2020.

Parameters of droplet bouncing

When a droplet falls from a high place and hits a solid substrate, solid–liquid contact electrification will occur, and then the subsequent electric output will be achieved through charge separation. Therefore, the contact area of the solid with a liquid affects the maximum charge exchanged by the droplet generator. There are many factors that affect the contact area of droplet-based nanogenerator devices, including droplet motion characteristics, surface roughness, wettability, ambient temperature, and humidity.[83–89] In this part, we focus on the influence of the droplet motion characteristics on the contact area. The three main parameters that determine the droplet motion are[85,89] the Weber number, Reynolds number and Ohnesorge number. The Weber number can be interpreted as the ratio of kinetic energy to the surface tension of a droplet:

$$\mathrm{We} = \rho v 2d/\gamma \quad (3)$$

where ρ, d, v, and γ, represent the density, diameter, impact velocity and surface tension of the droplet, respectively. It is generally believed that when We is lower than 1, surface tension plays the leading role. In this case, it is difficult for the droplets to spread out, resulting in a reduction in the solid–liquid contact area and charge. Deng *et al.* reported that when droplets with different Weber numbers hit the surface of SiO_2 modified by perfluorooctyltrichlorosilane (PFOTS), the amount of charge obtained is different, and the charge density is positively correlated with the Weber number (Fig. 4a).[90] The second factor is the Reynolds number, Re, which can be understood as the ratio of the power to the droplet viscosity:

$$\mathrm{R_e} = \rho v d/\mu \quad (4)$$

where ρ, d, v, and μ represent the density, diameter, impact velocity and dynamic viscosity of the droplet, respectively. It has been suggested that the behavior of water droplets can be determined using the following equation:

$$k = \mathrm{W_e}^{1/2} \times \mathrm{R_e}^{1/4} \quad (5)$$

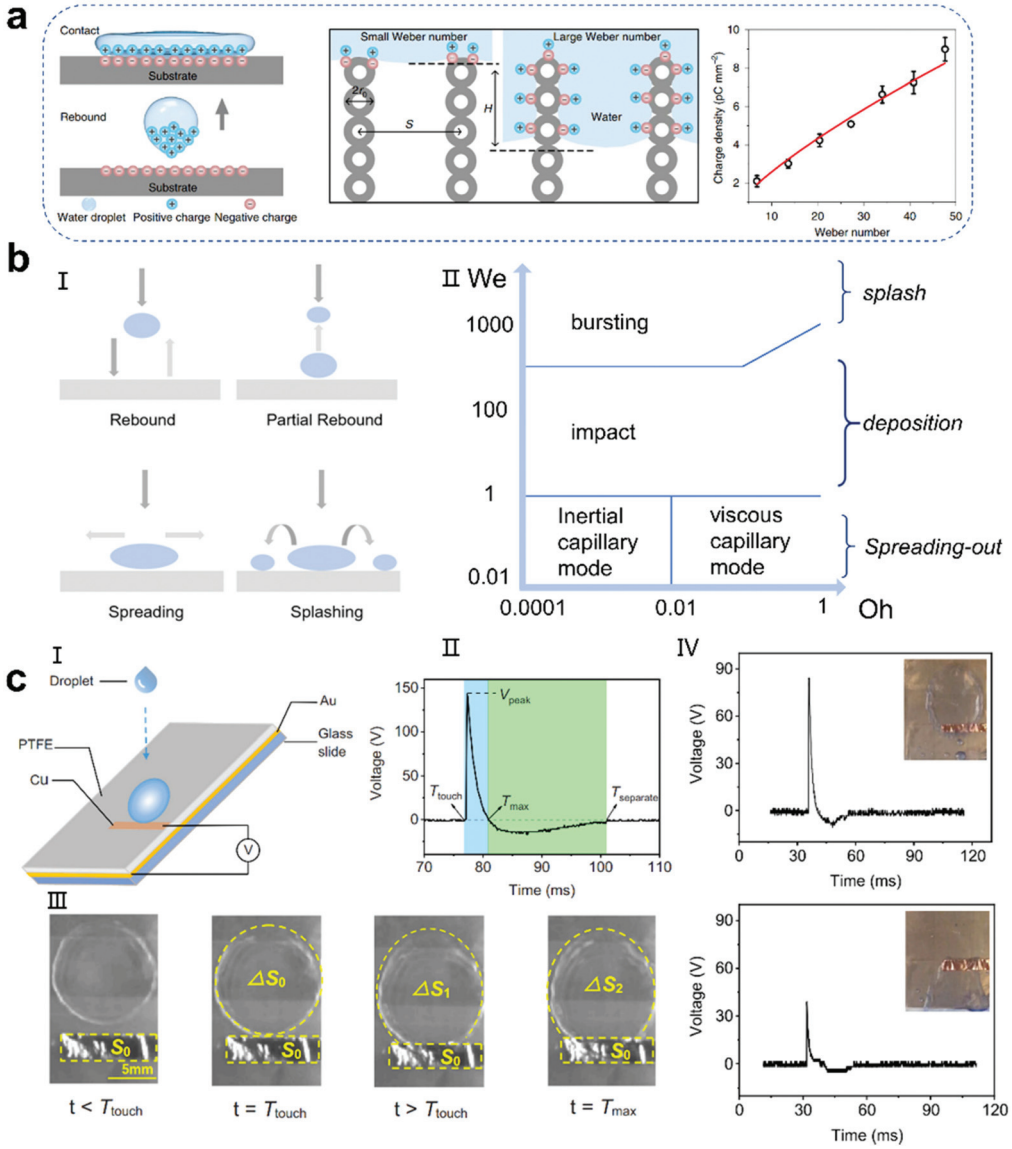

Fig. 4 Influence of bouncing droplets on the amount charges of droplets. (a) Schematic showing the charging of a superamphiphobic surface by droplet impact under different impact pressures and a plot of the charge density of the superamphiphobic surface as a function of the Weber number. These figures have been reproduced from ref. 90 with permission from Nature Publishing Group, Copyright 2019. (b) Impact of water droplets on a solid surface with different Re and We (I) and impact mode *versus* We and Oh(II). This figure has been reproduced from ref. 8 and 91 with permission from Elsevier and IOP Publishing, Copyright 2015 and 2018, respectively. (c) Schematic illustration of a droplet-based electricity generator (I). Voltage pulse generated by dropping one tap water droplet (II). Observation of the dynamics of the droplet with a high-speed camera (III). Voltage signals for the droplets released onto PTFE surface above and below the top electrodes, respectively (IV). These figures have been reproduced from ref. 92 with permission from Elsevier, Copyright 2021.

when k is much larger than the critical value K_c, droplet splashing will occur, and when k is much lower than K_c, droplets will deposit on the substrate (Fig. 4b-I).[8] For energy harvesting in a droplet nanogenerator, splashing and the deposition of droplets will cause the droplets to remain on the solid substrate, which is not conducive to the long-term stability of droplet-based nanogenerators. Therefore, only the appropriate droplet rebound can achieve a stable performance output. The third parameter is the Ohnesorge number (Oh), which is a dimensionless number that relates the viscous forces to inertial force and surface tension:

$$O_h = \mu/\sqrt{D_0\sigma\rho} = W_e^{1/2}/R_e \quad (6)$$

The motion mode determined by the interaction between We and Oh is shown in Fig. 4b-II.[91] When the droplet velocity is $1 \ll 1$, the droplet flow is controlled by the inertial or viscous capillarity force. With an increase in We, the droplet

motion will change to the deposition and splash mode. Although this is very useful to distinguish various types of motion, it does not consider all factors, such as surface wettability and roughness, and thus it needs to be used carefully. Moreover, the location of the droplets contacting the surface of the PTFE film should be seriously considered. Guo and colleagues found that dS/dt is the critical factor dominating the induced voltage. The area changes in the rate of the spreading droplet, dS/dt, revealed a curve similar to the voltage pulse, indicating that there is a close relationship between the induced voltage and dS/dt (Fig. 4c).[92] When the droplet has the largest spreading area and contacts the electrode, a higher voltage peak can be obtained because of the largest capacity for accommodating electrons.

3. Droplet-based nanogenerators for energy harvesting

Triboelectric nanogenerator based on droplets

Since the first solid–solid triboelectric nanogenerator was reported,[28] researchers have successfully fabricated various nanogenerators with different phases and materials based on contact electrification.[93–97] Liquid–solid TENGs follow a similar electrification principle as solid–solid TENGs (Fig. 5a).[97] When the liquid phase contacts the solid substrate, contact electrification occurs instantly. Normally, the charge is transferred from the liquid to solid, and then when the liquid slides over the solid surface, an electric field is established

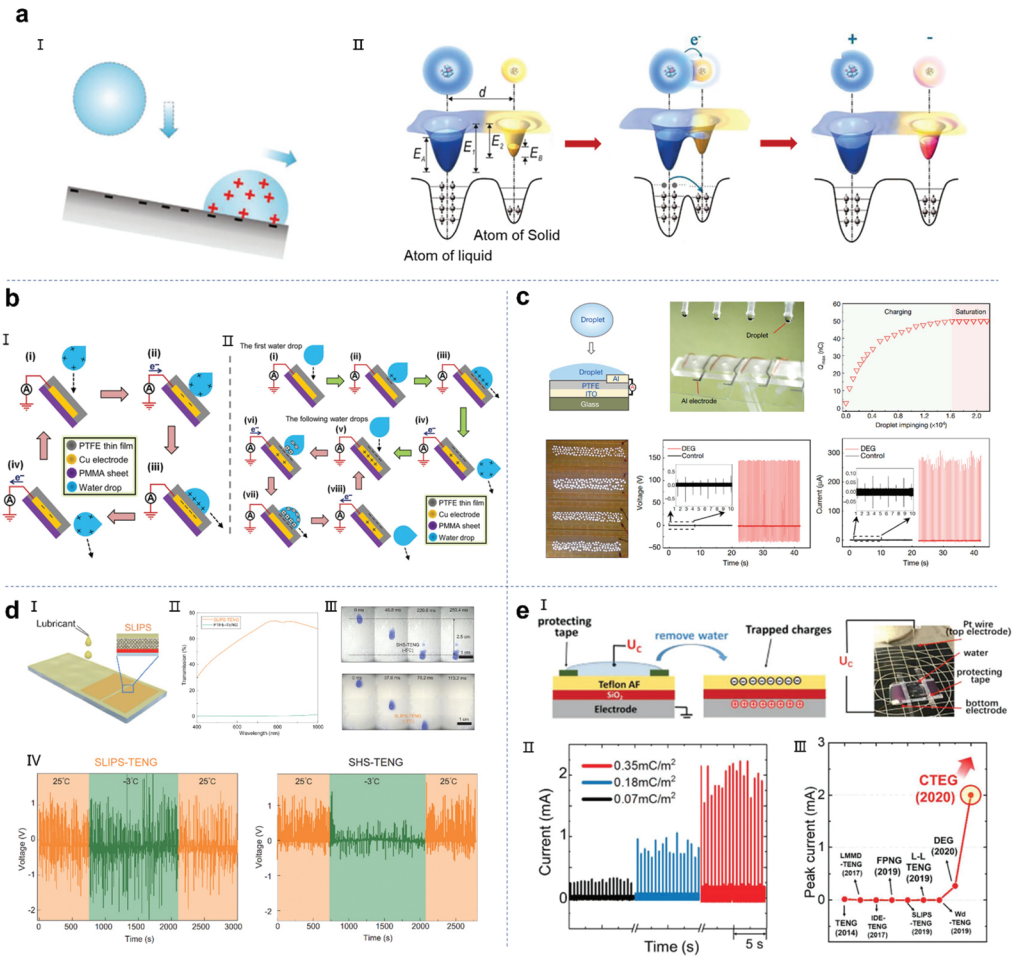

Fig. 5 Droplet nanogenerators based on the triboelectric effect. (a) Schematic illustration of the mechanism of a droplet-based TENG. These figures have been reproduced from ref. 39 and 97 with permission from Wiley-VCH and the American Chemical Society, Copyright 2020 and 2019, respectively. (b) Mechanism of a droplet-based TENG using a pre-charged droplet (I) or an uncharged droplet (II). These figures have been reproduced from ref. 18 with permission from Wiley-VCH, Copyright 2014. (c) Droplet-based electricity generator working based on the bulk effect. These figures have been reproduced from ref. 20 with permission from Nature Publishing Group, Copyright 2020. (d) SLIPS-TENG: SLIPS-TENG fabrication (I); optical transmittance between SLIPS (SLIPS-TENG) and PTFE (SHS-TENG) (II) and the time-dependent variation of the open-circuit voltage of SLIPS-TENG and SHS-TENG at 25 °C and −3 °C (III and IV), respectively. These figures have been reproduced from ref. 117 with permission from Oxford University, Copyright 2019. (e) Schematic of the h-EWCI method (I) and current generated by multiple falling droplets with an R_L of 2.2 kΩ (II) and energy landscape for the (injected) charge carriers of the h-EWCI method (III). These figures have been reproduced from ref. 62 with permission from Wiley-VCH, Copyright 2020.

between the electrodes because of electrostatic induction. When a load resistor or electrical appliance is connected, current will flow from one electrode to the other to balance the electric field formed by the separated charged surfaces. When the two charged surfaces contact again, the potential difference and the built-in electric field between the two electrodes will reverse, causing the current to flow in the opposite direction. Therefore, an alternating current (AC) is observed by repeating this cycle. In 2014, Wang *et al.* reported a nanogenerator based on solid–liquid triboelectricity between liquid droplets and PTFE film and proposed two solid–liquid electrical mechanisms (Fig. 5b).[18] The difference between the two modes is whether the droplets are pre-charged. 1. When the droplet is pre-charged with air or pipe friction, it is positively charged.[84,98–100] With the positively charged droplet approaching or contacting the PTFE film, a positive potential difference will occur between the Cu electrode and the ground. In the case of a short circuit, electrons are transferred from the ground to the copper electrode to balance the potential difference and eventually reach an electrical equilibrium state (Fig. 5b, III). As the droplet slides away, the electrons undergo reverse transfer, thus generating an alternating current signal. 2. If the water droplet is not pre-charged, when it contacts the PTFE film, the film surface will eventually be negatively charged and the droplet is positively charged due to the CE process. When the positively charged droplet leaves the film surface, the electrons will flow from the back electrode to the ground to achieve electrostatic equilibrium, resulting in a current flowing from the ground to the device. Given that the PTFE film, as a typical electret, can retain the triboelectric charge for a long time, another droplet falls and interacts with the negatively charged PTFE film and the negative charge on the PTFE film will attract the counter ions in the water droplet to form another electric double layer (EDL) with positive charge and establish a positive potential difference. Consequently, electrons will flow from the ground to the copper electrode until a new equilibrium is reached. This process produces an instantaneous positive current. When the water drops leave the PTFE film, there will be a negative potential difference between the copper electrode and the ground. The electrons will transfer from the copper electrode back to the ground, achieving a new balance. As the falling water droplets periodically contact the PTFE film, a continuous AC output will be obtained.

This electron transfer effect induced by the interface charge balance can be called the interface effect. Based on this interface effect, various structures and applications of droplet-based triboelectric nanogenerators have been widely reported, such as temperature sensors, force sensors, micro-liquid rate sensors and micro-gas rate sensors.[101–107] Although this interface effect can effectively harvest raindrop energy, the amount of charge transfer caused by a single droplet is very small, and thus the efficiency of this type of nanogenerator is not high. Recently, this situation was greatly improved. Wang and coworkers developed a device to harvest energy from impinging water droplets using a structure composed of a PTFE film on an indium tin oxide substrate and an aluminum electrode. They showed that the spreading of impinging water droplets on the device bridges the originally disconnected components into a closed-loop electrical system, transforming the traditional interface effect into a bulk effect (Fig. 5c).[20] Therefore, the instantaneous power density of the equivalent device limited by the interface effect increased by several orders of magnitude. This droplet generator exhibited a significantly enhanced energy harvesting efficiency of about 2.2%, and one drop of water could light 100 LED lights. Based on this breakthrough in the principle of the bulk effect, devices with different structures have been reported to achieve high electrical outputs.[108]

Although great progress has been made in the performance of droplet triboelectric nanogenerators, there are still some issues that need to be further improved. One of the main bottlenecks in the practical application of this type of droplet device is the rapid degradation of the physical and chemical properties of the interface material in harsh environments, such as high humidity, low temperature, mechanical stretching, bending and wear caused by dynamic motion.[109–113] Another major bottleneck is that the amount of charge generated by the droplets impinging the solid matrix material is not high, resulting in a low energy harvest efficiency.[114,115] To solve the problem of stability, researchers have applied slippery liquid-infused porous surfaces (SLIPS) to nanogenerator devices, designed and proposed SLIPS-TENG. Compared with traditional designs, the SLIPS-TENG exhibits many promising advantages, including optical transparency, configurability, self-cleaning, flexibility and power generation stability, even in harsh environments (Fig. 5d).[116,117] Compared with the traditional droplet TENGs, the SLIPS-TENG has higher transparency, can achieve a better self-cleaning performance at −5 °C and maintain a stable energy output at −3 °C. Another aspect of droplet-based nanogenerators that needs to be improved is how to increase the amount of charge contained in the solid material. In previous reports, the saturated polarization of PTFE was achieved by droplets hitting the PTFE film continuously. However, due to the limitation of the droplet impact position and depth, the bulk phase of PTFE cannot achieve saturation polarization. In a recent work, Mugele *et al.* reported that through electrowetting-assisted polarization (h-EWCI), a maximum charge density of 0.35 mC cm^{-2} and a milliampere-level current output were achieved (Fig. 5e), and the electricity conversion efficiency reached up to 11.8%.[62,118–120]

Tribovoltaic effect

Recently, Wang and colleagues discovered a new type of photovoltaic effect, where DC electric power is generated at the transition state when light is periodically illuminated at the interface of materials.[121] Based on this, they further found that when a p-type semiconductor slides over an n-type semiconductor, the energy "quantum" will be released due to the formation of new chemical bonds at the interface. The released energy can create electron–hole pairs at the interface.

Under the action of the built-in electric field at the semiconductor interface, the electron–hole pairs are further separated and move from one side to the other, generating a direct current in the external circuit. This phenomenon is similar to photovoltaic effect and is named the "tribovoltaic effect".[21,121–124]

The tribovoltaic effect can occur not only at the solid–solid interface, but also at the interface between an aqueous solution and a solid semiconductor, where the aqueous solution is considered a liquid semiconductor. As shown in Fig. 6a, Lin *et al.* used a conductive syringe needle to drag a deionized water (DI water) droplet to slide on the surface of silicon.[21] Fig. 6b shows the short-circuit current and open-circuit voltage between the conductive pin and the p-type silicon wafer. It was found that when deionized water droplets slide across the surface of p-type silicon, a positive current will be generated, which means that electrons move from the p-type silicon side to the deionized water side at the interface. In contrast, when deionized water droplets slide on the surface of n-type silicon, a negative current is generated and electrons move from the n-type silicon side to the deionized water side at the interface. It was found that the current direction is consistent with the direction of the built-in electric field at the water-silicon interface. In addition, Zheng and co-workers reported a study on the tribovoltaic effect of the liquid–solid interface under light irradiation (Fig. 6e).[121] The results showed that the tribocurrent between the DI water and the silicon wafer can be significantly enhanced by light irradiation, which is due to the increase in free electrons or holes at the interface under light irradiation. These studies showed that the tribovoltaic effect can obviously occur at the liquid–solid interface. Researchers have deeply studied the relevant mechanism. In the tribovoltaic effect of liquid–solid semiconductors, the energy of excited electron–hole pairs is also considered to come from the formation of chemical bonds at the interface. As shown in Fig. 6c, when water droplets slide across the semiconductor surface, some water molecules will contact the fresh surface to form chemical bonds and release energy. The released energy "quantum" is called "bindington". Fig. 6d shows the whole process of the tribovoltaic effect at the liquid–solid interface. When liquid and solid semiconductors contact each other, a built-in electric field will be generated at the interface due to the difference in the Fermi levels. At this time, if the liquid begins to slide on the surface of the solid semiconductor, the

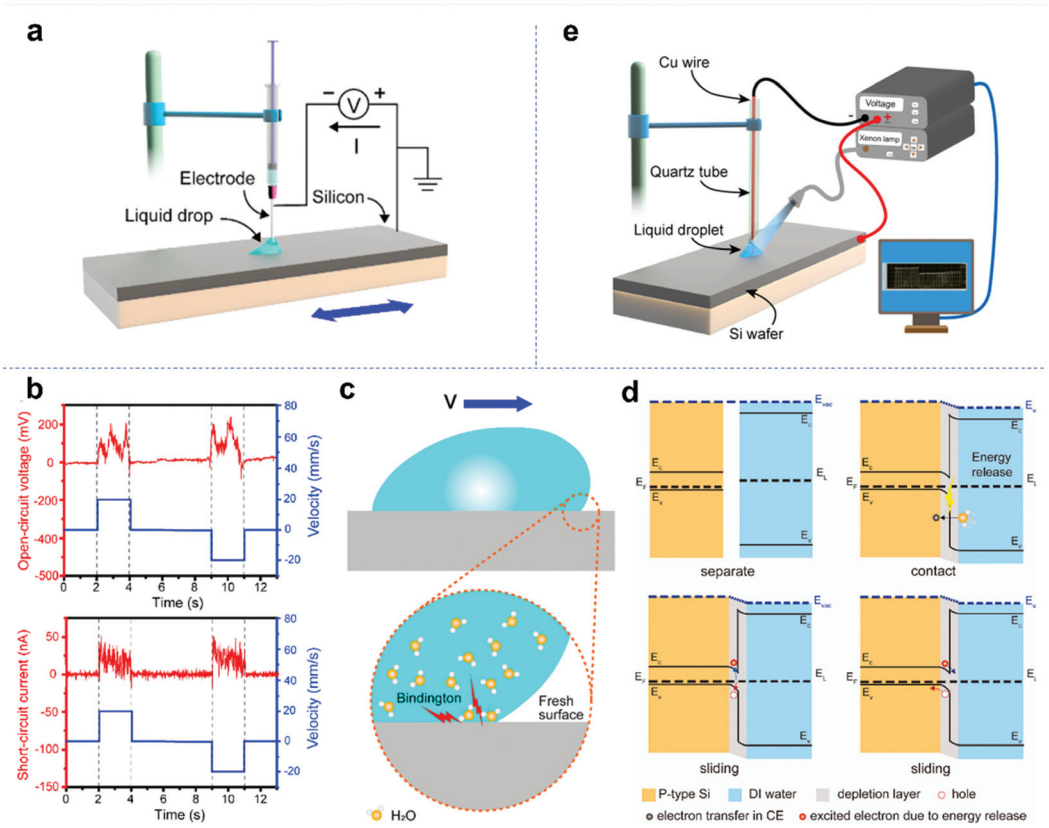

Fig. 6 Tribovoltaic effect at the liquid-semiconductor interface. (a) Setup of the tribovoltaic experiment and external circuit. (b) Oscillogram of tribo-voltage and tribo-current when a DI water droplet slides on a p-type silicon wafer. (c) Generation of the "bindington" at the interface between the sliding water and semiconductor. (d) Energy band diagram of the tribovoltaic effect at a liquid–solid junction. These figures have been reproduced from ref. 21 with permission from Elsevier, Copyright 2020. (e) Experimental setup for coupling the photovoltaic effect and tribovoltaic effect at the interface between DI water and an Si wafer. These figures have been reproduced from ref. 121 with permission from Elsevier, Copyright 2021.

junction will be released and electron–hole pairs will be created at the interface. Driven by the built-in electric field, the electron–hole pairs separate and move from one side to the other, generating a continuous DC current in the external load. The tribovoltaic effect offers a promising way to generate a DC current, which is very different from the droplet-based triboelectric nanogenerator. However, although it can be coupled with light to deliver more effective electron–hole separation, the tribo-voltage and tribo-current are still unsatisfactory. Thus, novel materials and devices for the tribovoltaic effect need to be further explored.[122–124]

Hydrovoltaic technology

Hydrovoltaic technology generates electricity through electrokinetic effects (Fig. 7a).[125] Electrokinetic phenomena driven by induced charge are widespread in the liquid–solid interface.[126] When a fluid contacts a charged/no-charge solid substrate, the ions in the fluid will be pre-adsorbed on the substrate and

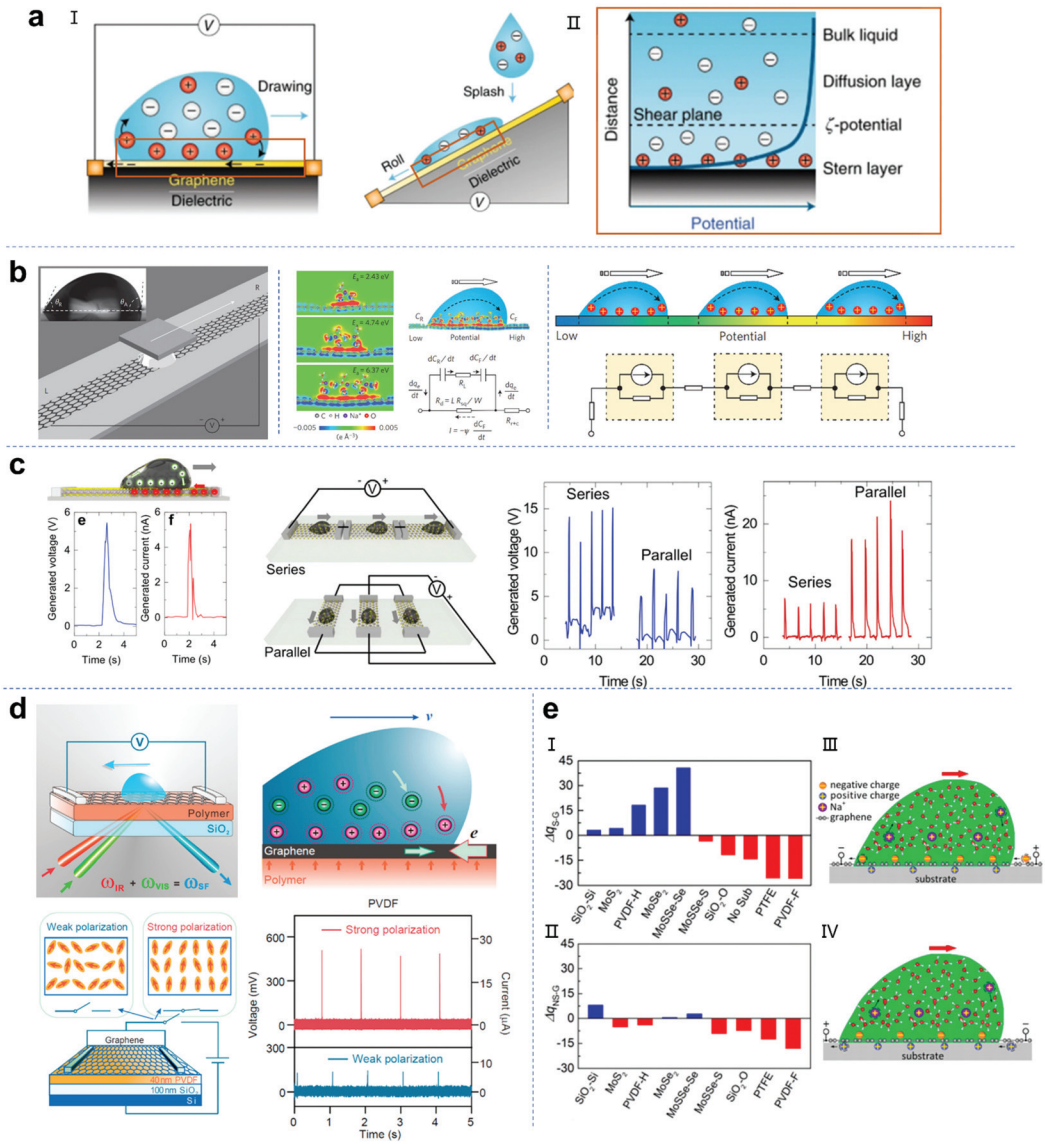

Fig. 7 Droplet nanogenerators based on hydrovoltaic technology. (a) Schematic illustration of the mechanism of hydrovoltaic technology. These figures have been reproduced from ref. 125 with permission from Nature Publishing Group, Copyright 2018. (b) Generating electricity by moving a droplet of ionic liquid along monolayer graphene on an SiO_2/Si wafer. These figures have been reproduced from ref. 17 with permission from Nature Publishing Group, Copyright 2014. (c) Generating electricity by moving ionic liquid droplets along monolayer MoS_2, series and parallel monolayer MoS_2 devices. These figures have been reproduced from ref. 130 with permission from Elsevier, Copyright 2020. (d) Sum-frequency vibrational spectroscopy for the mechanism study of electric power generation from ionic droplet motion on polymer-supported graphene. These figures have been reproduced from ref. 134 with permission from the American Chemical Society, Copyright 2018. (e) DFT calculations for the charge deviations in graphene or graphene-covered substrates in the presence (I) or absence (II) of Na^+ solution. Schematic illustration of the electricity generation process for n-type doped (III) and p-type doped (IV) graphene when a water droplet containing Na^+ moves on a graphene-covered substrate. These figures have been reproduced from ref. 135 with permission from Elsevier, Copyright 2021.

attract the counter ions in the droplets. Therefore, an electric double layer (EDL) will be formed at the interface. The EDL consists of a Stern layer close to the solid surface and a diffusion layer with rich counter-ions.[127–129] If an external force is applied to form a relative motion between the fluid and the solid substrate, the EDL will also have a corresponding movement to generate the electrokinetic effect. In 2014, Guo and co-workers successfully generated electricity by moving a droplet (containing NaCl) along graphene, with the maximum voltage and output power of 30 mV and 19.2 nW, respectively (Fig. 7b).[17] They proposed the mechanism of power generation by combining density functional theory calculation and EDL theory. When the NaCl aqueous solution contacts graphene, the Na^+ ions are preferentially adsorbed on graphene with an adsorption energy of over 2 eV, while the hydrated Cl^- anions repel graphene due to their negative adsorption energy. This physical adsorption promotes the formation of a solid–liquid EDL. When a droplet moves along the graphene, the charge balance of the EDL is broken. As the droplet moves on the graphene, ions are continuously adsorbed on the front end, which causes the pseudocapacitor to move forward and attract electrons on graphene. Simultaneously, the ions are desorbed at the back end of the droplet, discharging the pseudocapacitor and releasing electrons to graphene. Compared with the static state, the whole process leads to an increase/decrease in the electron density behind/in front of the moving droplet, resulting in a higher potential on the front side than on the back side. Therefore, a dynamic model was established. Although researchers have tried to improve the performance of graphene nanogenerators, the output voltage is still limited to ~100–400 mV. In a recent work, Ohno *et al.* reported that a large-area monolayer of MoS_2 prepared by the CVD process was used as a conductive substrate. When a drop of NaCl solution slides on the monolayer of MoS_2, an ultra-high voltage output of 5 V can be achieved (Fig. 7c).[130] In addition, they also fabricated parallel and series devices. The results showed that the polyethylene naphthalene (PEN) substrate enhances the sheet resistance and Na^+ ion adsorption of the MoS_2 layer and improves the output performance of the MoS_2-based droplet nanogenerator.

Although graphene-based conductive materials can convert the mechanical energy of a fluid flowing on the surface into electrical energy, at present, there is still a lack of understanding at the microscopic level of the underlying mechanism for optimizing the device structure to obtain a greater power output.[131–133] Recently, Tian *et al.* used sum-frequency vibrational spectroscopy (SFVS) to study the effects of solvated ions, graphene, the substrate surface, and water molecules on the aqueous solution/graphene/polymer interface (Fig. 7d).[134] The results showed that graphene does not have an effect of attracting ions, but only acts as a conductive substrate, which can be replaced by other conductive substrates with weak shielding effects. Furthermore, when graphene is on a substrate with stronger and denser surface dipoles, the attraction force to the interface ions can be increased, thereby achieving a greater power output. Using first-principles calculations, Guo and co-workers systematically studied the charge transfer between ionic solutions and different substrates (including polymers, silica and transition metal dichalcogenides) on a monolayer graphene coating.[135] This manner of polymer-supported graphene can achieve n-type or p-type doping of the graphene monolayer. Depending on the Bader charge analysis, the charge transfer and doping caused by the interaction between the Na^+ solution and substrates with graphene can be determined by calculating the charge deviation between the graphene coating and the independent graphene monolayer. As shown in Fig. 7e-I and II, $\Delta q_{S\text{-}G}$ and $\Delta q_{NS\text{-}G}$ represent the charge deviation of graphene in the presence and absence of Na^+ solution, respectively. A positive value indicates n-type doping and a negative value indicates p-type doping. Furthermore, through density functional theory (DFT) calculations, the authors proposed that monolayer graphene would be more deeply doped when Na^+ solution is present. Instead, when the solution is pure water, no obvious charge transfer occurs between the polymer and graphene. This proves that the synergistic effect of the Na^+ solution and the substrate can significantly enhance the doping of graphene and make graphene gain more holes/electrons. The results showed that both p-type doping and n-type doping can increase the attraction of Na^+ and accelerate the formation of an EDL interface.

Moreover, we further summarize the output power density of droplet-based nanogenerators in different manners. As shown in Fig. 8, the droplet-based TENG exhibits a much higher peak power density (W m^{-2}) than the other two types (nW). Furthermore, the droplet-based TENG generates an AC power in which a rectifier is needed to achieve a stable direct current output. In comparison, the tribovoltaic effect and hydrovoltaic technology can provide DC power, but their output power density needs to be further improved.

Other promising designs

Reverse electrowetting. The term electrowetting was first introduced in 1981 by G. Beni and S. Hackwood to describe an

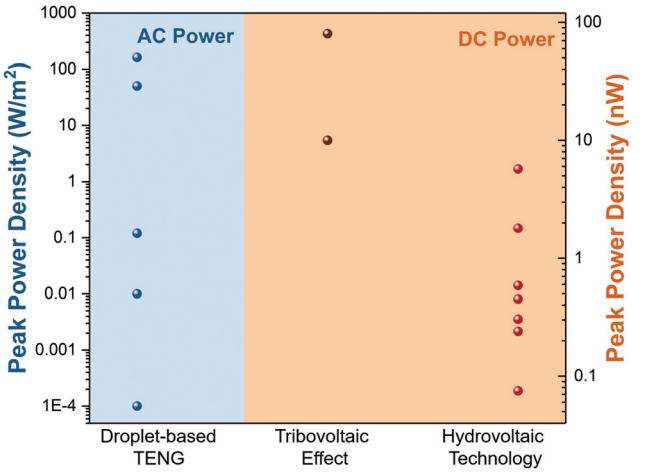

Fig. 8 Output power density of droplet-based nanogenerators in different manners.

effect proposed for designing a new type of display device.[136] In the 1990s, Berge and colleagues developed technology based on the electrowetting effect for spraying insulating layers on metal electrodes to avoid electrolysis of the conductive liquids.[137,138] The external bias voltage can change the electrostatic energy at the interface of the insulation layer of the charged droplet, resulting in a change in wettability. Therefore, the conductive droplets will spread on the insulating layer under an external bias. In 2011, Taylor and colleagues reported an innovative method to convert mechanical energy into electrical energy based on reverse electrowetting.[16] As shown in Fig. 9a, the electrodes are connected to an external power supply to provide a bias voltage for the device. When the droplet moves by external mechanical force, the overlapping area between the droplet and the electrode coated with the dielectric layer will decrease, resulting in a decrease in the charge at the liquid–solid interface. The extra charge flows through the circuit and generates electricity. Ideally, the liquid dielectric electrode interface can be regarded as a capacitor, and the current is caused by the change in capacitance. Generally, increasing the dielectric constant of the dielectric layer and decreasing its thickness can improve the maximum capacitance of the variable capacitor.[139] Although this method is very creative, there are still some problems. 1. The ultra-thin

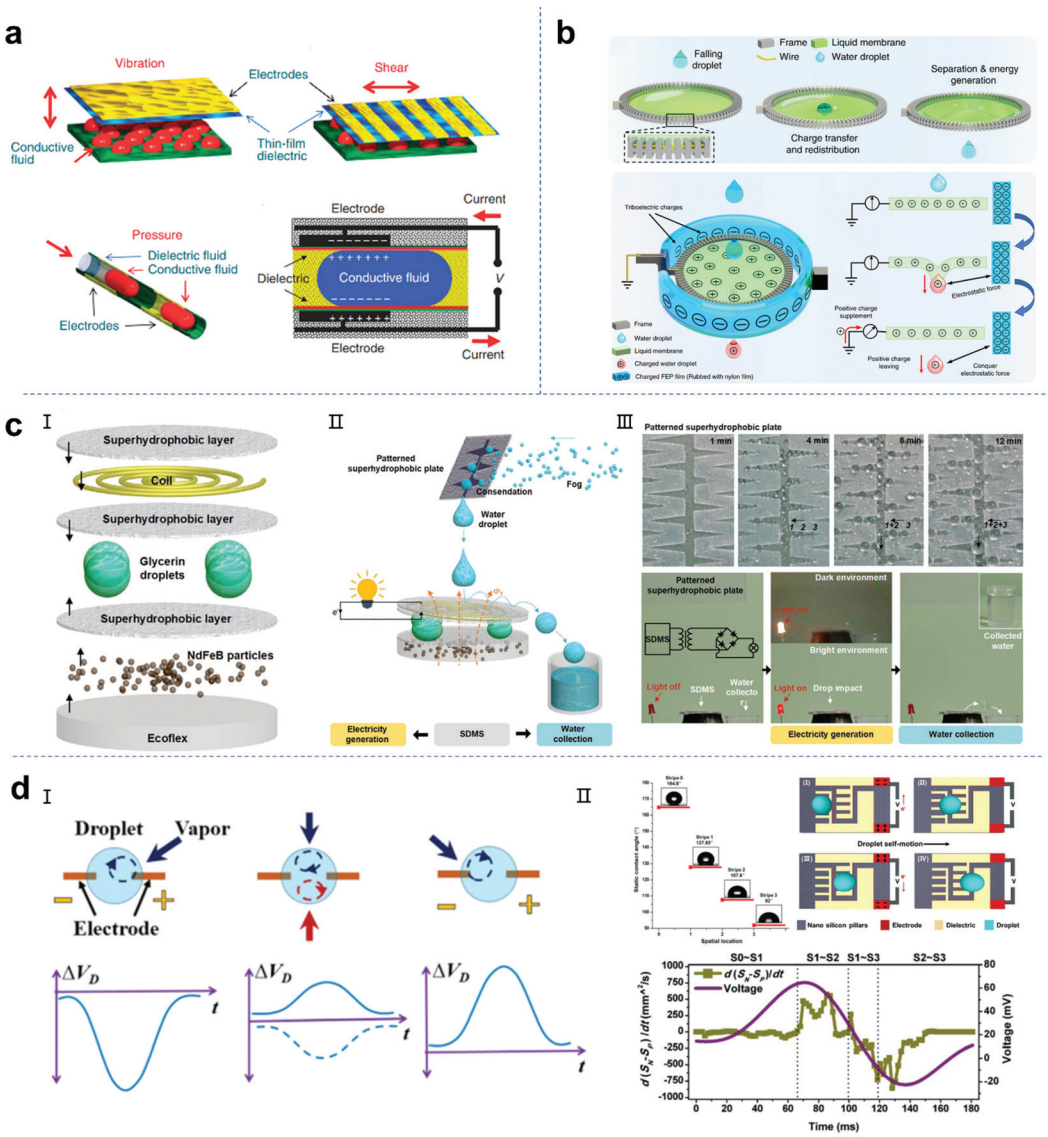

Fig. 9 Other promising designs of droplet-based nanogenerators. (a) Reverse electrowetting as a new approach for high-power energy harvesting. These figures have been reproduced from ref. 16 with permission from Nature Publishing Group, Copyright 2011. (b) Power generation from the interaction of a liquid droplet and a liquid membrane. These figures have been reproduced from ref. 19 with permission from Nature Publishing Group, Copyright 2019. (c) Magnetoelectric hybrid system based on super-hydrophobic droplets can generate electricity and collect water simultaneously. These figures have been reproduced from ref. 143 with permission from Wiley-VCH, Copyright 2020. (d) Self-motion droplets. These figures have been reproduced from ref. 144 and 145 with permission from the American Chemical Society, Copyright 2016 and 2018, respectively.

dielectric layer with a high dielectric constant easily decomposes even when a low bias is applied. 2. To promote the charge transfer at the interface, the wetting and dewetting cycle of the droplet on the dielectric layer should be fast and "smooth". The contact angle hysteresis and contact wire pinning hinder the response of the droplet to the bias voltage, resulting in a reduction in efficiency. Thus, to solve these problems, Yang *et al.* proposed the use of Al_2O_3 as an excellent dielectric material for a reverse driving nanogenerator and achieved an output power density of 11 mW cm^{-2}.[140] Compared with other processes, high-quality and ultra-thin Al_2O_3 dielectric layers can be obtained by atomic layer deposition, which provide a high dielectric constant and low leakage current density. Also, they are difficult to degrade, which is important for energy conversion.

Droplet and liquid membrane. Although increased efforts have been focused on droplet-based liquid–solid nanogenerators and related systems, there are few reports on the progress in energy harvesting based on the droplet-liquid (L–L) interface. In 2019, Chen and co-workers reported a triboelectric nanogenerator that can harvest energy based on the spontaneous charge redistribution between two pure liquids (Fig. 9b).[19] The droplet-liquid TENG functions by a droplet passing through the freely suspended liquid film (fluorinated ethylene propylene-FEP assisted polarization). Firstly, the FEP film is tribo-charged with a nylon film to make its surface negatively charged. Then, the pre-charged FEP film is placed around the liquid film through a frame ring, and the distance between them is about 1 cm to prevent discharge. The charged FEP film provides a high electric field to transfer the positive charge from the ground to the liquid film. The small gap between the FEP film and the liquid film can build a capacitor to accumulate charge. The working principle of the L–L nanogenerator is very similar to that of the traditional single-electrode triboelectric nanogenerator, which is shown in 1. The negative triboelectric charge on the FEP film forms an equilibrium system with the positively charged liquid film. 2. When a water droplet (without surface charge) contacts the liquid film, the positive charge on the liquid film will be redistributed between the water droplet and the liquid film. 3. Subsequently, the water droplets separate from the liquid membrane and take away a certain amount of positive charge, breaking the electrostatic balance. The charge needs to be transferred from the ground to the membrane to maintain the electrostatic balance. Therefore, the flow of electrons from the ground to the liquid film generates an energy output. A peak power of 137.4 nW can be achieved by a droplet falling (about 40 μL) through the pre-charged film.

Droplet-based magnetoelectric hybrid system. Water can store gravity and mechanical shock energy, which can be converted into electrical energy through hydroelectric power generation using electromagnetic generators. However, this type of electromagnetic generator is ponderous, bulky and unmovable, which is usually located near a dam, coast or river bank.[9,141,142] In addition, it is very difficult to generate electricity with traditional electromagnetic equipment in the case of water shortage such as no rain or fog.[20] Therefore, a miniature, novel and flexible electromagnetic hydroelectric converter that can harvest energy from tiny water droplets is a substitute for traditional hydroelectric equipment. Recently, Su and colleagues developed a small, portable, superhydrophobic droplet-based magnetoelectric hybrid system (SDMs), which can generate electricity and collect clean water simultaneously.[143] The SDM consists of three parts, namely, a superhydrophobic surface containing conductive coils, liquid droplets and superhydrophobic magnetic powder/Ecoflex substrate. Once a drop contacts the assembled system, its mechanical impact will change the magnetic flux through the coil, thereby generating electricity. The condensation of rain or fog will produce water droplets. In addition to generating electricity, the patterned superhydrophobic surfaces can also collect water from fog. A hybrid system composed of an SDM and cactus-like superhydrophobic paper cuts is shown in Fig. 9c. This superhydrophobic surface combined with soft magnetoelectric composite may improve and increase the energy harvesting function and provide a universal solution for the development of new resource-sustainable utilization systems.

Self-driving droplets. It has been demonstrated that the modulation of an electrical double layer at the liquid–solid interface offers promising potential to develop portable and efficient energy harvesting devices. The self-motion of a droplet can realize the movement of the electrical double layer to produce an electrokinetic effect to achieve energy harvesting.[126] It has been reported that a self-driving droplet induced by the Marangoni effect and interfacial tension changes can harvest energy.[144–146] Bandyopadhyay and colleagues found that a simple water droplet loaded with nanoparticles can sense volatile organic vapor and harvest energy simultaneously.[144] As shown in Fig. 8d-I, due to the formation of an electric double layer, the Cu electrode in water has a negative zeta potential. It is well known that the EDL will collapse with a high salt loading in the electrolyte, and therefore the effective zeta potential around the surface will be negligible. When organic vapor is introduced into the droplet, the surface tension of the droplet is changed. The rotation of the droplet due to the difference in surface tension is called the Marangoni effect. The strong rotational motion will disturb the EDL near the electrode, thereby partially recovering its zeta potential. It is important that the interference caused by the rotational movement is quite weak near the other electrode, and thus the recovery of the zeta potential is relatively small. Therefore, for the rotating droplet, they observed a limited drop in the potential ΔV_D on the Cu electrode (Fig. 9d-I-left). Moreover, control experiments were performed to corroborate this hypothesis, where it can be seen that the value and polarity of ΔV_D induced by the Marangoni effect are related to the direction of organic vapor introduction (Fig. 9d-I-middle-right). Besides the Marangoni effect, Wang and Zhou reported that the self-propelled motion of droplets driven by the surface wetting gradient can lead to reliable power generation (Fig. 9d-II).[145] The self-propelled transport of droplets on a solid surface usually requires a large wettability gradient to counter

the inherent contact angle (CA) hysteresis. The authors designed an anisotropic surface consisting of periodically patterned hydrophilic fences and an array of superhydrophobic nanopillars decorated between the grooves of the patterned fences. The static water CA was ~164.8°, 127.85°, 107.6° and 92°, respectively. When a droplet was placed on the chip with a large wettability gradient, the self-motion droplets produced the same electrokinetic effect to achieve energy generation. This interesting work demonstrates that a self-propelled 25 μL droplet can generate a peak current of 93.5 nA and a maximum output power of 2.4 nW.

4. Droplet-based nanogenerators for self-powered sensors

Self-powered physical sensors

Droplet-based nanogenerators with high output performances, cost effectiveness, flexibility and multiple material choices have attracted attention for physical sensing, including droplet flow rate, temperature, pressure and turbidity. Chen and co-workers reported a microfluidic sensor for detecting gas or liquid flow (Fig. 10a).[83] The detection range and sensitivity could be easily adjusted by changing the diameter of the capillary tube. Also, when the infusion rate varied from 3.14 to 62.8 μL s^{-1}, output signals of different frequencies were obtained (from 0.2 to 3.0 Hz), from which the interval of each droplet could be calculated. Conversely, the flux of the liquid medicine in a period of time can be calculated by counting the number of output peaks. Microfluidic sensors have important applications in self-powered mini full analysis systems. Zhou and colleagues reported a self-powered multimodal temperature and force sensor based on the reverse electrowetting effect and the thermo galvanic effect in a liquid droplet (Fig. 10b).[106] The deformation of the droplet and the temperature difference across the droplet can induce an alternating pulse voltage and a direct voltage, respectively, which are easy to separate/analyze and can be utilized to sense the external force and temperature simultaneously. In addition, an integrated display system that can derive information from external temperature/force concurrently was constructed. Combined with the advantages of excellent sensing performance and simple structure,

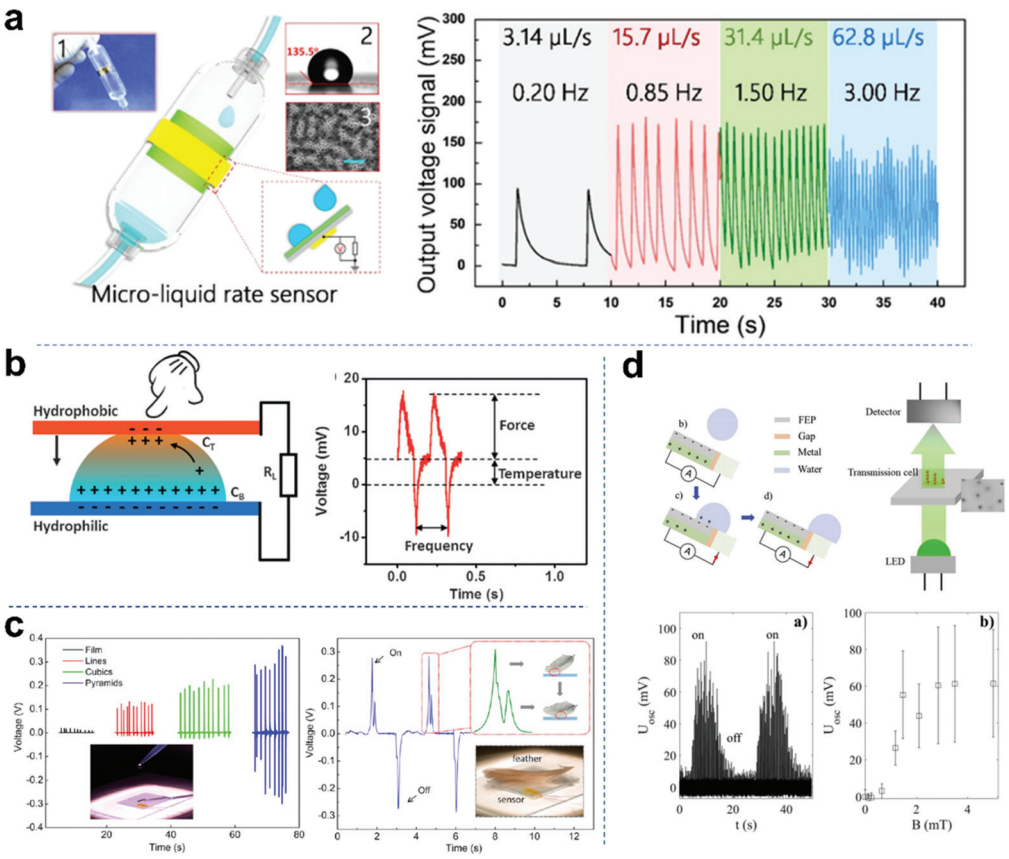

Fig. 10 Self-powered physical sensors based on droplet nanogenerators. (a) Configuration of micro-liquid rate sensor. These figures have been reproduced from ref. 83 with permission from the American Chemical Society, Copyright 2016. (b) Schematic structure and principle of the temperature and force sensor and the *U*–*T* curve of a droplet-based sensor when temperature and force coupled stimulation are applied. These figures have been reproduced from ref. 106 with permission from Wiley-VCH, Copyright 2016. (c) Performance of the pressure sensor device induced by a drop of water and a feather. These figures have been reproduced from ref. 25 with permission from the American Chemical Society, Copyright 2012. (d) Principle of a magnetic field-controlled turbidity sensor based on a droplet-powered light emitting diode. These figures have been reproduced from ref. 147 with permission from Elsevier, Copyright 2020.

the droplet sensor has promising applications in a wide range of intelligent electronics. Pressure sensors are one of the most commonly used sensors in industrial applications. They are widely used in various industrial automation fields. Pressure sensors with high precision and high sensitivity have always been the main goal. As shown in Fig. 10c, Fan *et al.* first measured the applied pressure induced by a drop of water (8 mg, ~3.6 Pa in pressure) using a TENG as a self-powered pressure sensor.[25] Furthermore, they also measured the response to the impact of a feather (20 mg, ~0.4 Pa in contact pressure), which corresponds to the low-end detection limit of 13 mPa. The sensor showed two opposite voltage signal curves, indicating the feather loading (on) and unloading (off) process. Recently, Helseth *et al.* developed a water droplet sensor and turbidity sensor based on a flow-through front surface electrode (Fig. 10d).[147] When water droplets pass through the polymer-covered metal surface, the sensor system generates a charge pumped from the back electrode to the front electrode. Then, it allows more charge transfer during each droplet impact than that induced by a single electrode mounted on the back of the polymer. Each drop of water will produce a flash in the light-emitting diode, which is detected by a silicon photodetector located at a certain distance. In addition, the proposed sensor system can be used to monitor the turbidity of liquid samples and continuously contact falling water droplets. When an axial magnetic field is applied, the magnetic beads form a chain, and the light transmittance decreases significantly. The observed average signal from the detector as a function of magnetic field B proved that the large fluctuations are caused by the changing signal generated by each droplet.

Self-powered chemical sensors

Chemical sensors can continuously detect and analyze specific molecules in the human body and surrounding environment. They have broad application prospects in human health and

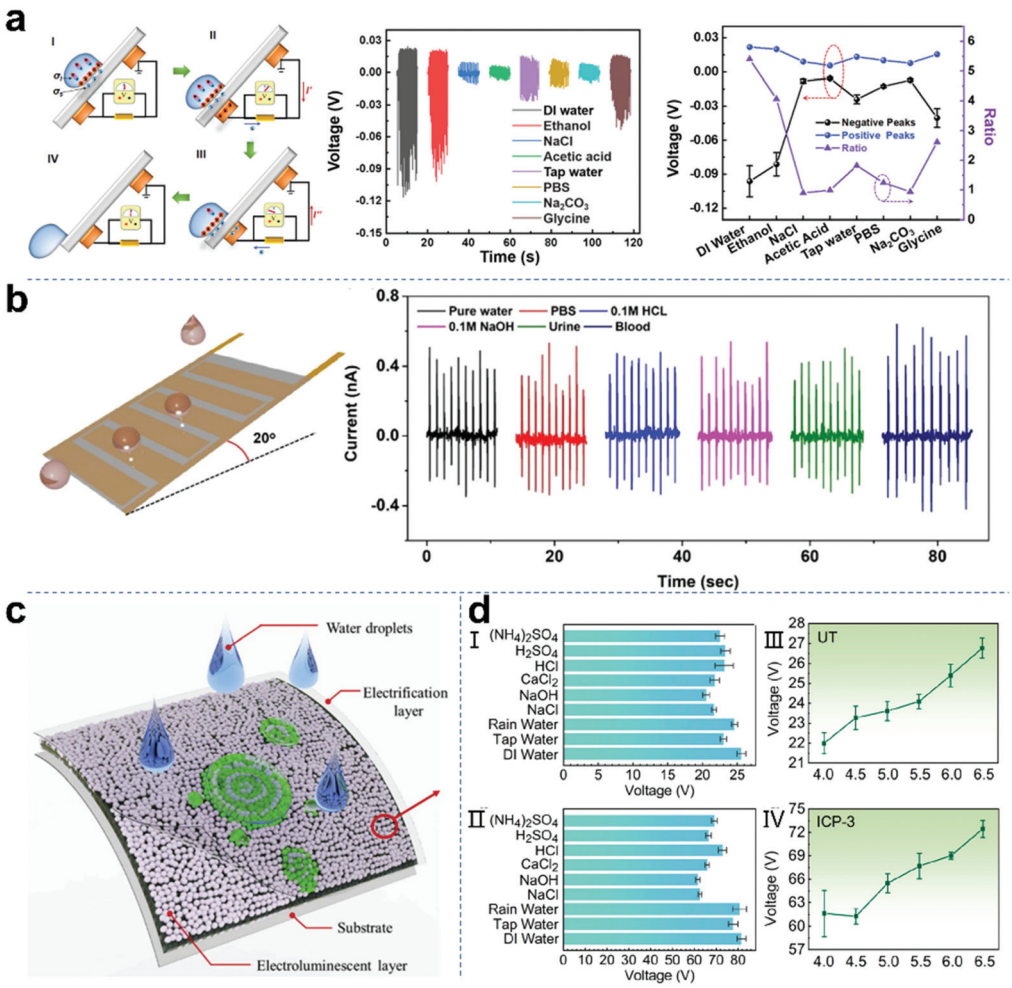

Fig. 11 Self-powered chemical sensors based on droplet nanogenerators. (a) Mechanism and sensing capabilities of a TE-based liquid sensor to different analytes. These figures have been reproduced from ref. 148 with permission from The Royal Society of Chemistry, Copyright 2021. (b) Schematic diagram of droplets rolling over a superhydrophobic TENG and the pulsed currents generated by six types of droplets. These figures have been reproduced from ref. 149 with permission from the American Chemical Society, Copyright 2020. (c) Schematic diagram of SL-TEL. These figures have been reproduced from ref. 150 with permission from Elsevier, Copyright 2020. (d) Output performance of a raindrop-TENG under different conditions. These figures have been reproduced from ref. 151 with permission from the American Chemical Society, Copyright 2021.

environmental protection. Self-powered chemical sensing based on droplet nanogenerators with the advantages of miniaturization, portability and rapidity is a promising method that can be applied to various fields in daily life. Wang and co-workers reported a self-powered triboelectric sensor for liquid chemical sensing based on liquid–solid contact electrification (Fig. 11a).[148] When the droplet passes across the tribo-negative sensor surface, the induced surface charge will be balanced with the electric double layer charge in the droplet. The competition between the bilayer charge and surface charge produces characteristic positive and negative voltage signals, which can be used as a "dual feature" for identifying compounds. This sensor showed obvious sensitivity to three amino acids (including glycine, lysine and phenylalanine) and several other inorganic and organic compounds dissolved in DI water. As shown in Fig. 11b, Yang *et al.* reported a superhydrophobic TENG and its biomedical applications as a droplet sensor.[149] The developed superhydrophobic TENG has many advantages in terms of simple fabrication, bendability, self-cleaning, self-adhesiveness, and high sensitivity, and is repellent not only to water but also to various solutions, including blood with a contact angle of 158.6°. The pulse current signals can be generated by six types of droplets rolling over the superhydrophobic TENG inclined at 20° from the horizontal plane. As a self-powered sensor, the developed prototypes of a drainage bottle droplet sensor and a smart intravenous injection monitor based on superhydrophobic liquid–solid TENGs can monitor the clinical drainage operation and intravenous infusion in real time, respectively. Furthermore, Zhu *et al.* proposed a novel solid–liquid electroluminescence (SL-TEL) based on the interfacial triboelectric field.[150] When a droplet hits the surface of the SL-TEL device, green electroluminescence with specific textures is emitted in two overlapping areas (Fig. 11c). The SL-TEL is essentially an electroluminescence device excited by changing the triboelectric field formed by the droplet impact or wave scouring. It relies on the intermediate triboelectric field to convert the mechanical energy of the liquid into visible light energy without consuming any electrical energy. The experimental results showed that the continuous liquid motion of droplets hitting the solid surface excites the corresponding dynamic series of electroluminescent patterns. The characteristics of the electroluminescence also reveal the properties of liquid and solid surfaces, such as the contour edge of liquid spreading and the capillary convergence (forward and backward) of liquid at the vertex, which can sense liquid leakage and display the dynamic information of droplet motion. Recently, Ping and co-workers reported a self-powered intelligent greenhouse system based on raindrop TENGs.[151] Actual rainwater usually contains various ions, such as SO_4^{2-}, NH_4^+, Ca^{2+}, NO_3^-, Na^+, and H^+. As shown in Fig. 11dI and II, the output voltage of the raindrop TENG with different liquids (DI water, tap water, 0.01 M NaCl, *etc.*) and natural rainwater was explored. Furthermore, the influence of rainwater with different pH values was also investigated. As shown in Fig. 11dIII and IV, the more acidic the solution, the worse the output performance of the raindrop TENG. This is because the concentration of H^+ in the solution increases as the acidity increases, resulting in an increase in the conductivity of the solution. This study contributes to the construction of sustainable and self-powered intelligent agriculture through various electronic devices in the era of the Internet of Agriculture.

5. Summary and perspective

As an environmentally friendly and sustainable power source, droplet-based nanogenerators have developed rapidly in the past few years as an effective means to harvest energy from the surrounding environment. Nevertheless, the output performance of a single droplet-based nanogenerator is at a relatively low level, which poses a challenge to the advancement of related fields. In this review, we briefly summarized the latest developments in droplet-based nanogenerators, focusing on droplet properties, energy harvesting and self-powered sensing based on different principles. The energy output of droplet nanogenerators is greatly affected by the properties and motion characteristics of droplets. Simultaneously, further improvement in the performance of droplet-based nanogenerators requires the coupling of their mechanism and structural characteristics. Although substantial progress has been made, various tasks and additional research still need to be completed to achieve a fundamental understanding and expand their potential applications. Some challenges and opportunities are summarized as follows:

Deepen the understanding of droplet properties for droplet-based nanogenerators

To improve the energy efficiency of DENGs, a large number of studies have been conducted to explore and develop new triboelectric materials. In addition, a triboelectric series based on different types of solid materials have been reported.[47,152] However, triboelectric solid materials are only part of the composition of droplet nanogenerators. How to achieve a large amount of charge transfer at the solid–liquid interface is an urgent problem to be solved. Although there are many studies on the surface roughness, topological structure and wettability of solids, there are few studies on the ability of droplets to be charged and stabilize the charge. Therefore, there is an urgent need to establish a triboelectric series of liquid molecules, which is not only conducive to the development of DENGs, but also brings a new Dawn to liquid–liquid triboelectric nanogenerators.

Design and optimization of robust droplet nanogenerators

At present, the efficiency of droplet nanogenerators is still too low to power some commonly used electronic devices. Specifically, the interaction between water and solid is very weak and limited to the surface layer of the materials. Therefore, each molecule or ion moving on the surface can only drive a few charged carriers. The optimization of the device layout and structural engineering, as well as the syn-

thesis of solid materials with a high specific surface area, high conductivity and strong water–solid interaction require further research. More importantly, droplet energy harvesting is usually carried out in an environment of high humidity, high salinity and low temperature. Therefore, it is necessary to design robust power generation devices in combination with engineering materials, surface wettability, fluid science and other fields.

Exploring hybrid energy conversion techniques

A variety of coupled generator modes needs to be explored to make up for the shortcomings of nanogenerators based on different principles. For example, triboelectric nanogenerators can generate a high-voltage pulse output, and hydrovoltaic technology devices can generate a stable direct current output, but the generated voltage and current signals are very weak compared with that of triboelectric nanogenerators. Therefore, how to effectively couple these two types of droplet nanogenerators to achieve high performance and stable output is a very promising topic. Simultaneously, the development of new droplet power generation devices, such as droplet tribovoltaic nanogenerators, droplet thermoelectric nanogenerators, novel droplet magnetoelectric nanogenerators, and even multi-field coupling power generation, will bring vigorous development in droplet-based nanogenerators.

Conflicts of interest

The authors declare no competing interests.

References

1 Z. L. Wang, *Nature*, 2017, **542**, 159–160.
2 H. Wang, Q. Zhu, Z. Ding, Z. Li, H. Zheng, J. Fu, C. Diao, X. Zhang, J. Tian and Y. Zi, *Nano Energy*, 2019, **57**, 616–624.
3 J. Tan, Y. Y. Zhao, X. Y. Yang, J. L. Duan, Y. D. Wang and Q. W. Tang, *J. Mater. Chem. A*, 2019, **7**, 5373–5380.
4 G. L. Stephens, J. Li, M. Wild, C. A. Clayson, N. Loeb, S. Kato, T. Lecuyer, P. W. Stackhouse Jr., M. Lebsock and T. Andrews, *Nat. Geosci.*, 2012, **5**, 691–696.
5 B. Dudley, *Stat. Rev.*, 2018, **6**, 00116.
6 Z. Wang, L. Tan, X. M. Pan, G. Liu, Y. H. He, W. C. Jin, M. Li, Y. M. Hu and H. S. Gu, *ACS Appl. Mater. Interfaces*, 2017, **9**, 28586–28595.
7 J. Ding, W. Q. Tao and S. K. Fan, *Nano Energy*, 2020, **70**, 104473.
8 M. A. Ilyas and J. Swingler, *Energy*, 2015, **90**, 796–806.
9 J. H. Lee, S. M. Kim, T. Y. Kim, U. Khan and S. W. Kim, *Nano Energy*, 2019, **58**, 579–584.
10 C. S. Wu, A. C. Wang, W. B. Ding, H. Y. Guo and Z. L. Wang, *Adv. Energy Mater.*, 2019, **9**, 1802906.
11 W. L. Liu, Z. Wang, G. Wang, G. L. Liu, J. Chen, X. J. Pu, Y. Xi, X. Wang, H. Y. Guo, C. G. Hu and Z. L. Wang, *Nat. Commun.*, 2019, **10**, 1426.
12 Z. L. Wang, T. Jiang and L. Xu, *Nano Energy*, 2017, **39**, 9–23.
13 S. W. Thomson, *Proc. R. Soc. London*, 1867, 1–10.
14 A. G. Marin, W. Hoeve, P. G. Sanchez, L. Shui, Y. Xie, M. A. Fontelos, J. C. T. Eijkel, A. van den Berg and D. Lohse, *Lab Chip*, 2013, **13**, 4503–4506.
15 R. Guigon, J. J. Chaillout, T. Jager and G. Despesse, *Smart Mater. Struct.*, 2008, **17**, 015039.
16 T. Krupenkin and J. A. Taylor, *Nat. Commun.*, 2011, **2**, 448.
17 J. Yin, X. M. Li, J. Yu, Z. H. Zhang, J. X. Zhou and W. L. Guo, *Nat. Nanotechnol.*, 2014, **9**, 378–383.
18 Z. H. Lin, G. Cheng, S. M. Lee, K. C. Pradel and Z. L. Wang, *Adv. Mater.*, 2014, **26**, 4690–4696.
19 J. H. Nie, Z. M. Wang, Z. W. Ren, S. Y. Li, X. Y. Chen and Z. L. Wang, *Nat. Commun.*, 2019, **10**, 2264.
20 W. H. Xu, H. X. Zheng, Y. Liu, X. F. Zhou, C. Zhang, Y. X. Song, X. Deng, M. Leung, Z. B. Yang, R. X. Xu, Z. L. Wang, X. C. Zeng and Z. K. Wang, *Nature*, 2020, **578**, 392–396.
21 S. Q. Lin, X. Y. Chen and Z. L. Wang, *Nano Energy*, 2020, **76**, 105070.
22 H. Yang, F. R. Fan, Y. Xi and W. Z. Wu, *EcoMat*, 2021, **3**, 12093.
23 H. Yang, F. R. Fan, Y. Xi and W. Z. Wu, *Adv. Sustainable Syst.*, 2020, **4**, 2000108.
24 J. J. Luo, Z. M. Wang, L. Xu, A. C. Wang, K. Han, T. Jiang, Q. S. Lai, Y. Bai, W. Tang, F. R. Fan and Z. L. Wang, *Nat. Commun.*, 2019, **10**, 1–9.
25 F. R. Fan, L. Lin, G. Zhu, W. Wu, R. Zhang and Z. L. Wang, *Nano Lett.*, 2012, **12**, 3109–3114.
26 S. H. Shin, Y. H. Kwon, Y. H. Kim, J. Y. Jung, M. H. Lee and J. Nah, *ACS Nano*, 2015, **9**, 4621–4627.
27 J. S. Chun, J. W. Kim, W. Jung, C. Y. Kang, S. W. Kim, Z. L. Wang and J. M. Baik, *Energy Environ. Sci.*, 2015, **8**, 3006–3012.
28 F. R. Fan, Z. Q. Tian and Z. L. Wang, *Nano Energy*, 2012, **1**, 328–334.
29 W. G. Kim, D. W. Kim, W. Tcho, J. K. Kim, M. S. Kim and Y. K. Choi, *ACS Nano*, 2021, **15**, 258–287.
30 X. J. Li, L. Q. Zhang, Y. G. Feng, X. L. Zhang, D. A. Wang and F. Zhou, *Adv. Funct. Mater.*, 2019, **29**, 1903587.
31 Y. Wang, S. G. Gao, W. H. Xu and Z. K. Wang, *Adv. Funct. Mater.*, 2020, **30**, 1908252.
32 F. R. Fan, W. Tang and Z. L. Wang, *Adv. Mater.*, 2016, **28**, 4283–4305.
33 K. Q. Wang and J. J. Li, *J. Mater. Chem. A*, 2021, **9**, 8870–8895.
34 S. Chatterjee, S. R. Burman, I. Khan, S. Saha, D. Choi, S. Lee and Z. H. Lin, *Nanoscale*, 2020, **12**, 17663–17697.
35 A. Chen, C. Zhang, G. Zhu and Z. L. Wang, *Adv. Sci.*, 2020, **7**, 2000186.
36 Y. K. Liu and C. G. Hu, *Nanoscale*, 2020, **12**, 20118–20130.
37 G. Zhu, B. Peng, J. Chen, Q. S. Jing and Z. L. Wang, *Nano Energy*, 2015, **14**, 126–138.

38 W. Tang, B. D. Chen and Z. L. Wang, *Adv. Funct. Mater.*, 2019, **29**, 1901069.
39 W. H. Xu, Y. X. Song, R. X. Xu and Z. K. Wang, *Adv. Mater. Interfaces*, 2020, **8**, 2000670.
40 J. H. Nie, Z. W. Ren, L. Xu, S. Q. Lin, F. Zhan, X. Y. Chen and Z. L. Wang, *Adv. Mater.*, 2020, **32**, 1905696.
41 A. G. Banpurkar, Y. Sawane, S. M. Wadhai, C. U. Murade, I. Siretanu, D. Endeb and F. Mugele, *Faraday Discuss.*, 2017, **199**, 29–47.
42 M. D. Sosa, M. L. M. Ricci, L. L. Missoni, D. H. Murgida, A. Canneva, N. B. D. Accorsode and R. M. Negri, *Soft Matter*, 2020, **16**, 7040–7051.
43 B. J. Kirby and E. F. Hasselbrink, *Electrophoresis*, 2004, **25**, 187–202.
44 T. Preocanin, A. Selmani, P. Lindqvist-Reis, F. Heberling, N. Kallay and J. Lutzenkirchen, *Colloids Surf., A*, 2012, **412**, 120–128.
45 A. Barisic, J. Lutzenkirchen, G. Lefevre and T. Begovic, *Colloids Surf., A*, 2019, **579**, 123616.
46 J. Lutzenkirchen, T. Preocanin and N. Kallay, *Phys. Chem. Chem. Phys.*, 2008, **10**, 4946–4955.
47 H. Y. Zou, Y. Zhang, L. T. Guo, P. H. Wang, X. He, G. Z. Dai, H. W. Zheng, C. Y. Chen, A. C. Wang, C. Xu and Z. L. Wang, *Nat. Commun.*, 2019, **10**, 1427.
48 J. Luo, L. Xu, W. Tang, T. Jiang, F. R. Fan, Y. Pang, L. Chen, Y. Zhang and Z. L. Wang, *Adv. Energy Mater.*, 2018, **8**, 1800889.
49 L. F. Chen, Q. F. Shi, Y. J. Sun, T. Nguyen, C. Lee and S. Soh, *Adv. Mater.*, 2018, **30**, 1802405.
50 N. Zhang, H. J. Gu, K. Y. Lu, S. M. Ye, W. H. Xu, H. X. Zheng, Y. X. Song, C. R. Liu, J. W. Jiao, Z. K. Wang and X. F. Zhou, *Nano Energy*, 2021, **82**, 105735.
51 Z. L. Wang, L. Lin, J. Chen, S. M. Niu and Y. L. Zi, *Triboelectric Nanogenerators*, Springer International Publishing, Berlin, 2016.
52 T. A. L. Burgo, F. Galembeck and G. H. Pollack, *J. Electrost.*, 2016, **80**, 30–33.
53 L. Liu, Q. Shi, J. S. Ho and C. Lee, *Nano Energy*, 2019, **66**, 104167.
54 A. Kaya and Y. Yukselen, *J. Hazard. Mater.*, 2005, **120**, 119–126.
55 L. M. Vane and G. M. Zang, *J. Hazard. Mater.*, 1997, **55**, 1–22.
56 J. L. Snyder, J. Getpreecharsawas, D. Z. Fang, T. R. Gaborski, C. C. Striemer, P. M. Fauchet, D. A. Borkholder and J. L. McGrath, *Proc. Natl. Acad. Sci. U. S. A.*, 2013, **110**, 18425–18430.
57 R. B. M. Schasfoort, S. Schlautmann, J. Hendrikse and A. v. d. Berg, *Science*, 1999, **286**, 942–945.
58 E. J. v. d. Wouden, T. Heuser, D. C. Hermes, R. E. Oosterbroek, J. G. E. Gardeniers and A. v. d. Berg, *Colloids Surf., A*, 2005, **267**, 110–116.
59 A. Plecis, J. Tazid, A. Pallandre, P. Martinhon, C. Deslouis, Y. Chen and A. M. Haghiri-Gosnet, *Lab Chip*, 2010, **10**, 1245–1253.
60 X. Wu, P. R. Rajasekaran and C. R. Martin, *ACS Nano*, 2016, **10**, 4637–4643.
61 P. Jin, H. Mukaibo, L. P. Horne, G. W. Bishop and C. R. Martin, *J. Am. Chem. Soc.*, 2010, **132**, 2118–2119.
62 H. Wu, N. Mende, S. V. D. Ham, L. L. Shui, G. F. Zhou and F. Mugele, *Adv. Mater.*, 2020, **32**, 2001699.
63 Y. J. Sun, X. Huang and S. Soh, *Chem. Sci.*, 2015, **6**, 3347–3353.
64 J. Park, Y. J. Yang, S. H. Kwon and Y. S. Kim, *J. Phys. Chem. Lett.*, 2015, **6**, 745–749.
65 D. Choi, D. W. Kim, D. Yoo, K. J. Cha, M. La and D. S. Kim, *Nano Energy*, 2017, **36**, 250–259.
66 S. B. Jeon, M. L. Seol, D. Kim, S. J. Park and Y. K. Choi, *Adv. Electron. Mater.*, 2016, **2**, 1600006.
67 X. Yang, S. Chan, L. Wang and W. A. Daoud, *Nano Energy*, 2018, **44**, 388–398.
68 M. Han, B. Yu, G. Qiu, H. Chen, Z. Su, M. Shi, B. Meng, X. Cheng and H. Zhang, *J. Mater. Chem. A*, 2015, **3**, 7382–7388.
69 L. E. Helseth and X. D. Guo, *Langmuir*, 2015, **31**, 3269–3276.
70 Z. Huang, Y. N. Yao, W. Li and B. Hu, *Anal. Chim. Acta*, 2019, **1050**, 105–112.
71 L. J. Diorazio, D. R. Hose and N. K. Adlington, *Org. Process Res. Dev.*, 2016, **20**, 760–773.
72 V. G. Drozin, *J. Colloid Sci.*, 1955, **10**, 158–164.
73 A. Jones and K. Thong, *J. Phys. D: Appl. Phys.*, 1971, **4**, 1159.
74 Q. Guo, V. Singh and S. H. Behrens, *Langmuir*, 2010, **26**, 3203–3207.
75 K. H. Lim, Y. J. Sun, W. C. Lim and S. Soh, *J. Am. Chem. Soc.*, 2020, **142**, 21004–21016.
76 Z. Y. Li, Y. Long and J. W. Zhong, *Nano Energy*, 2021, **81**, 105618.
77 L. Pan, J. Wang, P. Wang, R. Gao, Y. C. Wang, X. Zhang, J. J. Zou and Z. L. Wang, *Nano Res.*, 2018, **11**, 4062–4073.
78 J. Wang, Z. Wu, L. Pan, R. Gao, B. Zhang, L. Yang, H. Guo, R. Liao and Z. L. Wang, *ACS Nano*, 2019, **13**, 2587–2598.
79 X. Li, J. Tao, X. Wang, J. Zhu, C. Pan and Z. L. Wang, *Adv. Energy Mater.*, 2018, **8**, 1800705.
80 http://ch301.cm.utexas.edu/imfs/#polar/dipole-moment.html.
81 https://www.doitpoms.ac.uk/tlplib/dielectrics/dielectric_constant.php.
82 A. Ghosh, M. Yoshida, K. Suemori, H. Isago, N. Kobayashi, Y. Mizutani, Y. Kurashige, I. Kawamura, M. Nirei, O. Yamamuro, T. Takaya, K. Iwata, A. Saeki, K. Nagura, S. Ishihara and T. Nakanishi, *Nat. Commun.*, 2019, **10**, 4210.
83 J. Chen, H. Guo, J. Zheng, Y. Huang, G. Liu, C. Hu and Z. L. Wang, *ACS Nano*, 2016, **10**, 8104–8112.
84 H. Cho, J. Chung, G. Shin, J. Y. Sim, D. S. Kim, S. Lee and W. Hwang, *Nano Energy*, 2019, **56**, 56–64.
85 S. N. Zhang, J. Y. Huang, Z. Chen, S. Yang and Y. K. Lai, *J. Mater. Chem. A*, 2019, **7**, 38–63.
86 S. L. Feng, J. Delannoy, A. Malod, H. X. Zheng, D. Quere and Z. K. Wang, *Sci. Adv.*, 2020, **6**, eabb4540.
87 H. Y. Dai, Z. C. Dong and L. Jiang, *Sci. Adv.*, 2020, **6**, eabb5528.

88 D. Z. Shen, W. W. Duley, P. Peng, M. Xiao, J. Y. Feng, L. Liu, G. S. Zou and Y. N. Zhou, *Adv. Mater.*, 2020, **32**, 2003722.
89 S. Schiaffino and A. A. Sonin, *Phys. Fluids*, 1997, **9**, 3172–3187.
90 Q. Q. Sun, D. H. Wang, Y. Li, J. H. Zhang, S. J. Ye, J. X. Cui, L. Q. Chen, Z. K. Wang, H. J. Butt, D. Vollmer and X. Deng, *Nat. Mater.*, 2019, **18**, 936–941.
91 R. Guigon, J. J. Chaillout, T. Jager and G. Despesse, *Smart Mater. Struct.*, 2018, **17**, 015038.
92 X. Wang, S. M. Fang, J. Tan, T. Hu, W. C. Chu, J. Yin, J. X. Zhou and W. L. Guo, *Nano Energy*, 2021, **80**, 105558.
93 W. Zhong, L. Xu, F. Zhan, H. M. Wang, F. Wang and Z. L. Wang, *ACS Nano*, 2020, **14**, 10510–10517.
94 L. L. Zhou, D. Liu, Z. H. Zhao, S. X. Li, Y. B. Liu, L. Liu, Y. K. Gao, Z. L. Wang and J. Wang, *Adv. Energy Mater.*, 2020, **10**, 2002920.
95 L. H. Li, S. W. Gao, M. M. Hao, X. Q. Yang, S. J. Feng, Z. H. Wang, L. L. Li, S. Q. Wang, S. Wang, F. Q. Sun, Y. Li, Y. Y. Bai, Z. K. Wang and T. Zhang, *Nano Energy*, 2021, **85**, 105970.
96 J. J. Luo, F. R. Fan, T. Jiang, Z. W. Wang, W. Tang, C. P. Zhang, M. M. Liu, G. Z. Cao and Z. L. Wang, *Nano Res.*, 2015, **8**, 3934–3943.
97 Z. L. Wang and A. C. Wang, *Mater. Today*, 2019, **30**, 34.
98 B. Ravelo, F. Duval, S. Kane and B. Nsom, *J. Electrost.*, 2011, **69**, 473–478.
99 T. Takahashi, *Rev. Geophys.*, 1973, **11**, 903–924.
100 S. K. Banerji and S. R. Lele, *Nature*, 1932, **13**, 2226.
101 B. D. Chen, W. Tang, C. He, T. Jiang, L. Xu, L. P. Zhu, G. Q. Gu, J. Chen, J. J. Shao, J. Luo and Z. L. Wang, *Adv. Mater. Technol*, 2017, **3**, 1700229.
102 A. K. M. Newaz, D. A. Markov, D. Prasai and K. I. Bolotin, *Nano Lett.*, 2012, **12**, 2931–2935.
103 B. Zhang, L. Zhang, W. Deng, L. Jin, F. Chun, H. Pan, B. Gu, H. Zhang, Z. Lv, W. Yang and Z. L. Wang, *ACS Nano*, 2017, **11**, 7440–7446.
104 X. Zhang, Y. Zheng, D. Wang and F. Zhou, *Nano Energy*, 2017, **40**, 95–106.
105 W. Kim, D. Choi, J. Y. Kwon and D. Choi, *J. Mater. Chem. A*, 2018, **6**, 14069–14076.
106 K. Liu, Y. S. Zhou, F. Yuan, X. B. Mo, P. H. Yang, Q. Chen, J. Li, T. P. Ding and J. Zhou, *Angew. Chem., Int. Ed.*, 2016, **55**, 15864–15868.
107 N. Zhang, H. J. Gu, H. X. Zheng, S. M. Ye, L. Kang, C. Huang, K. Y. Lu, W. H. Xu, Q. Q. Miao, Z. K. Wang, J. Zhang and X. F. Zhou, *Nano Energy*, 2020, **73**, 104748.
108 H. J. Gu, N. Zhang, Z. Y. Zhou, S. M. Ye, W. J. Wang, W. H. Xu, H. X. Zheng, Y. X. Song, J. W. Jiao, Z. K. Wang and X. F. Zhou, *Nano Energy*, 2021, **87**, 106218.
109 C. Clanet, C. B. E. Guin and D. Richard, *J. Fluid Mech.*, 2004, **517**, 199–208.
110 X. Tian, T. Verho and R. H. Ras, *Science*, 2016, **352**, 142–143.
111 S. Moulinet and D. Bartolo, *Eur. Phys. J. E*, 2007, **24**, 251–260.
112 K. K. Varanasi, T. Deng and J. D. Smith, *Appl. Phys. Lett.*, 2010, **97**, 234102.
113 D. Richard, C. Clanet and D. Quere, *Nature*, 2002, **417**, 811.
114 Y. Liu, L. Moevius and X. Xu, *Nat. Phys.*, 2014, **10**, 515–519.
115 H. Wu, N. Mendel, D. V. D. Ende, G. G. Zhou and F. Mugele, *Phys. Rev. Lett.*, 2020, **125**, 078361.
116 W. H. Xu and Z. K. Wang, *Joule*, 2020, **4**, 2527–2531.
117 W. H. Xu, X. F. Zhou, C. L. Hao, H. X. Zheng, Y. Liu, X. T. Yan, Z. B. Yang, M. Leung, X. C. Zeng, R. X. Xu and Z. K. Wang, *Natl. Sci. Rev.*, 2019, **6**, 540–550.
118 N. Mendel, H. Wu and F. Mugele, *Adv. Funct. Mater.*, 2020, **31**, 2007872.
119 X. M. Li, H. M. Tian, J. Y. Shao, Y. C. Ding, X. L. Chen, L. Wang and B. H. Lu, *Adv. Funct. Mater.*, 2016, **26**, 2994–3002.
120 H. Y. Zou, G. Z. Dai, A. C. Wang, X. G. Li, S. L. Zhang, W. B. Ding, L. Zhang, Y. Zhang and Z. L. Wang, *Adv. Mater.*, 2020, **32**, 1907249.
121 M. Zheng, S. Lin, Z. Tang, Y. Feng and Z. L. Wang, *Nano Energy*, 2021, **83**, 105810.
122 Z. Zhang, D. D. Jiang, J. Q. Zhao, G. X. Liu, T. Z. Bu, C. Zhang and Z. L. Wang, *Adv. Energy Mater.*, 2020, **10**, 1903713.
123 J. Meng, Z. H. Guo, C. X. Pan, L. Y. Wang, C. Y. Chang, L. W. Li, X. Pu and Z. L. Wang, *ACS Energy Lett.*, 2021, **6**, 2442–2450.
124 M. L. Zheng, S. Q. Lin, L. Xu, L. P. Zhu and Z. L. Wang, *Adv. Mater.*, 2020, **32**, 2000928.
125 Z. H. Zhang, X. M. Li, J. Yin, Y. Xu, W. W. Fei, M. M. Xue, Q. Wang, J. X. Zhou and W. L. Guo, *Nat. Nanotechnol.*, 2018, **13**, 1109–1119.
126 S. Wall, *Curr. Opin. Colloid Interface Sci.*, 2010, **15**, 119–124.
127 L. P. Block, *Astrophys. Space Sci.*, 1978, **55**, 59–83.
128 S. L. Carnie and G. M. Torrie, *Adv. Chem. Phys.*, 2007, **56**, 141–253.
129 D. C. Grahame, *Chem. Rev.*, 1947, **41**, 441–501.
130 A. S. Aji, R. Nishi, H. Ago and Y. Ohno, *Nano Energy*, 2020, **68**, 104370.
131 S. S. Kwak, S. Lin, J. H. Lee, H. Ryu, T. Y. Kim, H. Zhong, H. Chen and S. W. Kim, *ACS Nano*, 2016, **10**, 7297–7302.
132 Q. Tang, X. Wang, P. Yang and B. He, *Angew. Chem., Int. Ed.*, 2016, **55**, 5243–5246.
133 G. Shi, J. Liu, C. Wang, B. Song, Y. Tu, J. Hu and H. Fang, *Sci. Rep.*, 2013, **3**, 3436.
134 S. S. Yang, Y. D. Su, Y. Xu, Q. Wu, Y. B. Zhang, M. B. Raschke, M. X. Ren, Y. Chen, J. L. Wang, W. L. Guo, Y. R. Shen and C. S. Tian, *J. Am. Chem. Soc.*, 2018, **140**, 13746–13752.
135 H. F. Cai, Y. F. Guo and W. L. Guo, *Nano Energy*, 2021, **84**, 105939.
136 G. Beni and S. Hackwood, *Appl. Phys. Lett.*, 1981, **38**, 207.
137 B. Berge, *C.R Acad. Sci. Paris Ser II*, 1993, **317**, 157–163.
138 F. Mugele and J. C. Baret, *J. Phys.: Condens. Matter*, 2005, **17**, R705.

139 S. Paria, S. K. Si, S. K. Karan, A. K. Das, A. Maitra, R. Bera, L. Halder, A. Bera, A. Dea and B. B. Khatua, *J. Mater. Chem. A*, 2019, **7**, 3979–3991.
140 H. Yang, S. Hong, B. Koo, D. Lee and Y. B. Kim, *Nano Energy*, 2017, **31**, 450–455.
141 M. F. Xiong, J. Lin, S. L. Wang, K. Gaw and P. S. L. Parida, *Adv. Energy Mater.*, 2017, **7**, 1701243.
142 J. H. Zhang, Y. Li and X. Hao, *Nanotechnology*, 2020, **31**, 215401.
143 Z. Ma, J. W. Ai, Y. S. Shi, K. Wang and B. Su, *Adv. Mater.*, 2020, **32**, 2006839.
144 M. Bhattacharjee, V. Pasumarthi, J. Chaudhuri, A. K. Singh, H. Nemade and D. Bandyopadhyay, *Nanoscale*, 2016, **8**, 6118–6128.
145 C. R. Liu, J. Sun, Y. Zhuang, J. Wei, J. Li, L. X. Dong, D. F. Yan, A. Hu, X. F. Zhou and Z. K. Wang, *Nanoscale*, 2018, **10**, 23164–23169.
146 L. D. Zhang, Y. H. Yuan, X. X. Qiu, T. Zhang, Q. Chen and X. H. Huang, *Langmuir*, 2017, **33**, 12609–12615.
147 L. E. Helseth, *Nano Energy*, 2020, **73**, 104809.
148 Z. H. Ying, Y. Long, F. Yang, Y. T. Dong, J. Li, Z. Y. Zhang and X. D. Wang, *Analyst*, 2021, **146**, 1656.
149 S. M. Hu, Z. J. Shi, R. Z. Zheng, W. L. Ye, X. Gao, W. W. Zhao and G. Yang, *ACS Appl. Mater. Interfaces*, 2020, **12**, 40021–40030.
150 X. J. Zhao, S. Y. Kuang, Z. L. Wang and G. Zhu, *Nano Energy*, 2020, **75**, 104823.
151 Q. Zhang, C. M. Jiang, X. J. Li, S. F. Dai, Y. B. Ying and J. P. Ping, *ACS Nano*, 2021, **15**, 12314–12323.
152 M. Seol, S. Kim, Y. Cho, K. E. Byun, H. Kim, J. Kim, S. K. Kim, S. W. Kim, H. J. Shin and S. Park, *Adv. Mater.*, 2018, **30**, 1801210.